Available online at www.sciencedirect.com

ScienceDirect

Underground Space 26 (2026) 175–196

www.keaipublishing.com/undsp

Research Paper

Probabilistic seismic response analysis of tunnel linings considering coupled rock mass property and earthquake excitation uncertainties

Xiancheng Mei [a,b,c], Jiajun Wu [a,c,*], Baiyi Li [b], Zhen Cui [a,c], Chong Yu [a,c], Qian Sheng [a,c], Jian Chen [a,c]

[a] State Key Laboratory of Geomechanics and Geotechnical Engineering Safety, Institute of Rock and Soil Mechanics, Chinese Academy of Sciences, Wuhan 430071, China

[b] State Key Laboratory of Intelligent Construction and Healthy Operation and Maintenance of Deep Underground Engineering, Xuzhou 221116, China

[c] University of Chinese Academy of Sciences, Beijing 100049, China

Received 14 July 2025; received in revised form 29 August 2025; accepted 31 August 2025
Available online 19 November 2025

Abstract

Tunnel lining seismic performance is significantly influenced by the spatial variability of geological parameters and the uncertainty of earthquake excitation factors, which are conventionally treated in isolation. This study proposes a novel probabilistic framework that integrates random field theory with an enhanced Clough–Penzien spectrum to concurrently model both uncertainty sources. The approach offers a more realistic and integrated assessment of seismic risk for tunnels under complex geological and loading conditions. The case analysis of a railway project reveals that considering both spatial variability of rock mass and uncertainty in seismic excitation leads to significant increases in internal forces and their variability, with mean values rising up to 278.9% and coefficients of variation (COV) up to 262.8%, compared to single-factor random analyses. The non-normal distribution of responses under seismic uncertainty, combined with the broader dispersion from rock variability, necessitates integrating both random factors for reliable seismic performance assessment of tunnels. Parametric studies demonstrate spectral parameters, including initial circular frequency (ω_0), equivalent damping ratio (ξ_0), and peak acceleration (a_{max}), significantly influence results: increasing ω_0 and ξ_0 markedly reduces both the mean and COV of lining mechanical response-by up to 83.5% and 82.5%, respectively-potentially underestimating failure risk and underscoring the need to adopt lower-bound values in design for enhanced safety. Meanwhile, a_{max} positively correlates with mean structural response, while variability in internal forces follows distinct trajectories; moreover, the interaction between rock spatial variability and seismic uncertainty raises failure probabilities by 3%–38%, emphasizing the necessity of integrating both randomness sources, especially in high-intensity seismic regions.

Keywords: Tunnel lining structure; Spatial variability; Random earthquake excitation; Random field; Clough–Penzien power spectrum; Random dynamic response

1 Introduction

The global proliferation of transportation infrastructure has led to a substantial increase in tunnel construction traversing seismically active regions (L. Wang et al., 2024; Mei et al., 2023; Cui et al., 2024). These underground structures face significant seismic hazards due to the prevalence of high-magnitude earthquakes in such areas.

* Corresponding author at: State Key Laboratory of Geomechanics and Geotechnical Engineering Safety, Institute of Rock and Soil Mechanics, Chinese Academy of Sciences, Wuhan 430071, China.
E-mail address: wujiajun21@mails.ucas.ac.cn (J. Wu).
Peer review under the responsibility of Tongji University

https://doi.org/10.1016/j.undsp.2025.08.001

Historical seismic events, including the 1923 Kanto (Japan), 2004 Niigata (Japan), 1999 Chi-Chi (Taiwan, China), and 2008 Wenchuan (China) earthquakes, have demonstrated the vulnerability of tunnel linings to seismic forces, resulting in the consequences of catastrophic structural failures and substantial economic losses (Wang et al., 2021; Chen et al., 2023; Yao et al., 2024; Singh et al., 2018). These documented cases underscore the critical need for comprehensive seismic reliability assessment of tunnel linings. Traditional deterministic methods, which rely on deterministic earthquake excitation mean property values, fail to adequately account for uncertainties during earthquake events, leading to incomplete assessments. A probabilistic analysis that considers geological and earthquake excitation uncertainties is essential for an aseismic performance evaluation of tunnel linings.

The seismic performance of tunnel linings is profoundly affected by the spatial variation of surrounding rock mass properties. Natural sedimentary processes induce significant spatial heterogeneity in rock properties across both horizontal and vertical dimensions (Li et al., 2024; Khosravi-Hajivand & Johari, 2024), introducing considerable uncertainty in rock mass parameter characterization. This geological variability has prompted extensive research into its engineering implications, particularly for slope stability (Zhang et al., 2015; Ding et al., 2023; Jiang et al., 2015; Renani et al., 2019; Johari & Rahmati, 2019; Johari & Fooladi, 2022), foundation bearing capacity (Wu et al., 2019; Jerez et al., 2024; Li et al., 2015; Johari & Talebi, 2021), and settlement analysis (Alibeikloo et al., 2022; Johari et al., 2019; Fenton & Griffiths, 2002; Zhang et al; 2023; Zhang et al; 2024; Dong et al., 2024; Johari & Sabzi, 2017). The tunneling community has particularly focused on this phenomenon (Napoli et al., 2021; Huang et al., 2017; Chen et al., 2019). Tunnel dynamic analyses have also advanced significantly, with Wu et al. (2024) developing a dimension-reduction spectral representation method for efficient simulation of soil property variability in seismic reliability assessments. Studies by Zhang et al. (2025) on station structures and Wang et al. (2022) on liquefiable soils have collectively demonstrated the critical importance of accounting for the spatial variability of rock mass properties in tunnel engineering, particularly for seismic performance evaluation.

The dynamic response analysis and seismic safety evaluation of structures must account for the inherent variability and uncertainty in earthquake excitations. The spectral representation (SR) method has become a fundamental approach for simulating random seismic motions since Housner's (1947) pioneering work modeling earthquakes as stochastic processes. This method is particularly valuable for engineering applications due to its ability to accurately capture key ground motion characteristics, including amplitude variations, duration effects, and spectral properties, while maintaining rigorous theoretical foundations for modeling fully nonstationary seismic processes (Sun et al., 2024; Huang & Chen, 2009; Pang et al., 2018a). Over the past decades, SR method has proven effective in generating artificial earthquake excitations for structural analysis. For instance, Pang et al. (2018b) applied the SR-random function method to assess the safety of high concrete-faced rockfill dams under pulse-like and non-pulse-like seismic loads. Similarly, Xu et al. (2024) integrated SR with rockfill softening and shear strength variability to develop a framework for dam slope stability evaluation. Ji et al. (2021) combined SR with the Newmark method to analyze slope displacements, highlighting the substantial impact of seismic uncertainty on stability. Additionally, Chen and Li (2025) employed SR for stochastic dynamic analysis and reliability assessment of reinforced concrete structures under stochastic ground motions. A key consensus from these studies is that seismic uncertainty critically affects structural performance, and SR method provides an effective means to assess stochastic dynamic responses. However, research on tunnel structures remains limited, particularly regarding their seismic behavior and safety evaluation under stochastic earthquake conditions.

The present study develops an analytical framework for evaluating the stochastic response of tunnel lining structures that addresses critical limitations in current research by concurrently incorporating the spatial variability of rock mass properties and earthquake excitation randomness. While existing studies have typically examined these uncertainty sources in isolation or relied on oversimplified deterministic assumptions, this approach integrates random field theory for characterizing rock mass spatial variability with an improved Clough–Penzien (C–P) power spectrum model that properly accounts for nonstationary ground motion characteristics through random function methodology. The dynamic response of the mechanical behavior of the lining is then rigorously assessed through Monte Carlo Simulation (MCS), overcoming the common simplification of using deterministic or single-random-factor analyses. A systematic investigation of key seismic parameters, including initial circular frequency (ω_0), equivalent damping ratio (ξ_0), and peak acceleration ($a_{\max}$), further addresses the current lack of parametric sensitivity studies in tunnel seismic design. The methodology and findings presented herein contribute to more reliable performance predictions for underground structures by advancing beyond the limitations of prevailing deterministic or partial-probabilistic approaches.

2 Methodology

2.1 Random field theory

Rock mass behavior is fundamentally governed by mineral composition, stress history, and burial depth (Ching & Phoon, 2013a; Cao & Wang, 2014). Significant property variations exist both between lithological units and within homogeneous rock types, a phenomenon termed spatial variability. This inherent heterogeneity critically influences deformation mechanisms and failure patterns, making its

proper characterization essential for seismic design of tunnel lining structures. Random field theory (Vanmarcke, 1983) has become the standard approach for quantifying such spatial variations. Auto-correlation functions (ACFs) play a pivotal role in random field applications by establishing spatial relationships between geological parameters. While field investigations provide valuable data, they often fail to fully capture geological complexity due to practical constraints. Consequently, theoretical ACFs have been widely adopted (Phoon et al., 2003; Luo et al., 2018), with the two-dimensional squared exponential ACF emerging as the most prevalent model due to its computational efficiency and empirical validity.

$$\rho(\tau_x, \tau_y) = \exp\left[-\pi\sqrt{\left(\frac{\tau_x}{\delta_h}\right)^2 + \left(\frac{\tau_y}{\delta_v}\right)^2}\right], \tag{1}$$

where τ_x and τ_y are the horizontal and vertical distances between any two points in the random field; δ_h and δ_v are the horizontal and vertical scale of fluctuation (SOF), respectively. Accurate quantification of SOFs presents significant challenges in field applications due to the requirement for dense, localized measurements. To address this limitation, this study employs the maximum likelihood estimation (MLE) methodology (Ching et al., 2011) as an efficient solution for SOF determination under data-constrained conditions.

these parameters is grounded in the fundamental consistency of spatial variability patterns observed across geotechnical properties, as noted by Fenton et al. (2005). This consistency arises from shared geological formation processes and subsequent stress-weathering histories that collectively influence the spatial distribution of various geomechanical properties. The approach proves particularly valuable in engineering practice, where comprehensive field data for all parameters are typically unavailable.

σ_{ci} can be represented as a spatially variable field $\{\sigma_{ci}(x_i, y_i, z_i): i = 1,\cdots,n\}$, where (x_i, y_i, z_i) is the coordinate of location for the i-th rock core, and n is the total number of data points. To ensure physically meaningful positive values during stochastic sampling, all geotechnical parameters are modeled using lognormal distributions. The mean value $\mu_{\ln(\sigma_{ci})}$ and standard deviation $\sigma_{\ln(\sigma_{ci})}$ of $\ln(\sigma_{ci}(x,y,z))$ can be estimated as

$$\mu_{\ln(\sigma_{ci})} \approx \frac{1}{n}\sum_{i=1}^{n} \ln\left[\sigma_{ci}(x_i, y_i, z_i)\right], \tag{2}$$

$$\sigma_{\ln(\sigma_{ci})} \approx \sqrt{\frac{1}{n}\sum_{i=1}^{n} \ln\left\{\left[\sigma_{ci}(x_i, y_i, z_i)\right] - \mu_{\ln(\sigma_{ci})}\right\}^2}. \tag{3}$$

Assuming the SOF of the two-horizontal direction (x, y) are identical to δ_h, the covariance matrix of $\ln(\sigma_{ci}(x,y,z))$ is as follows:

$$\sum(\delta_h, \delta_v) = \sigma^2_{\ln(\sigma_{ci})}\begin{bmatrix} 1 & \exp\left(-2\sqrt{\left(\frac{\Delta h_{1,2}}{\delta_h}\right)^2 + \left(\frac{\Delta z_{1,2}}{\delta_v}\right)^2}\right) & \cdots & \exp\left(-2\sqrt{\left(\frac{\Delta h_{1,n}}{\delta_h}\right)^2 + \left(\frac{\Delta z_{1,n}}{\delta_v}\right)^2}\right) \\ \exp\left(-2\sqrt{\left(\frac{\Delta h_{2,1}}{\delta_h}\right)^2 + \left(\frac{\Delta z_{2,1}}{\delta_v}\right)^2}\right) & 1 & \cdots & \exp\left(-2\sqrt{\left(\frac{\Delta h_{2,n}}{\delta_h}\right)^2 + \left(\frac{\Delta z_{2,n}}{\delta_v}\right)^2}\right) \\ \vdots & \vdots & & \vdots \\ \exp\left(-2\sqrt{\left(\frac{\Delta h_{n,1}}{\delta_h}\right)^2 + \left(\frac{\Delta z_{n,1}}{\delta_v}\right)^2}\right) & \exp\left(-2\sqrt{\left(\frac{\Delta h_{n,2}}{\delta_h}\right)^2 + \left(\frac{\Delta z_{n,2}}{\delta_v}\right)^2}\right) & \cdots & 1 \end{bmatrix}, \tag{4}$$

This methodology establishes a practical approach for estimating SOFs from limited uniaxial compressive strength (σ_{ci}) field data, with the derived correlation characteristics being extendable to simulate random fields of other rock mechanical parameters. The transferability of

where $\Delta h_{i,j} = \sqrt{(x_i - x_j)^2 + (y_i - y_j)^2}$, $\Delta z_{i,j} = |z_i - z_j|$ are the horizontal and vertical distances, respectively, between the i-th and j-th rock cores. The likelihood function $L\{\delta_h, \delta_v | \ln[\sigma_{ci}(x_i, y_i, z_i)] : i = 1, \cdots, n\}$ of δ_h and δ_v is

$$L\{\delta_{\mathrm{h}},\delta_{\mathrm{v}}|\ln[\sigma_{ci}(x_i,y_i,z_i)]:i=1,\cdots,n\}$$
$$=\frac{1}{(2\pi)^{n/2}\sqrt{\det\left(\sum(\delta_{\mathrm{h}},\delta_{\mathrm{v}})\right)}}\exp\left\{-\frac{1}{2}\begin{bmatrix}\ln[\sigma_{ci}(x_1,y_1,z_1)]-\mu_{\ln(\sigma_{ci})}\\ \ln[\sigma_{ci}(x_2,y_2,z_2)]-\mu_{\ln(\sigma_{ci})}\\ \vdots\\ \ln[\sigma_{ci}(x_n,y_n,z_n)]-\mu_{\ln(\sigma_{ci})}\end{bmatrix}^{\mathrm{T}}\times\sum(\delta_h,\delta_v)^{-1}\begin{bmatrix}\ln[\sigma_{ci}(x_1,y_1,z_1)]-\mu_{\ln(\sigma_{ci})}\\ \ln[\sigma_{ci}(x_2,y_2,z_2)]-\mu_{\ln(\sigma_{ci})}\\ \vdots\\ \ln[\sigma_{ci}(x_n,y_n,z_n)]-\mu_{\ln(\sigma_{ci})}\end{bmatrix}\right\}. \tag{5}$$

The maximum value of $L\{\delta_{\mathrm{h}},\delta_{\mathrm{v}}\ln[\sigma_{ci}(x_i,y_i,z_i)]:i=1,\cdots,n\}$ represents the maximum likelihood estimate, which serves as the optimal solution for δ_{h} and δ_{v}.

Bringing the results of δ_{h} and δ_{v} into Eq. (1) can get the theoretical ACF of the project. Based on this, the lognormal random field G can be obtained by the Karhunen–Loeve (K–L) expansion method:

$$G=\sum_{t=1}^{M_k}\sqrt{\lambda_t}\xi_t\varphi_t(x), \tag{6}$$

where ξ_t is a set of independent standard normal distribution random variables; λ_t and $\varphi_t(x)$ are the eigenvalues and eigenfunctions of the ACF, respectively; M_k is the number of terms of the series expansion.

In summary, the random field of rock parameter X can be generated by the mean value μ_X, coefficient of variation COV_X(coefficient of variation: standard deviation/mean), and SOF_X ($\delta_{\mathrm{h}X}$, $\delta_{\mathrm{v}X}$). Calculate the mean value and standard deviation of the logarithm of X random field by

$$\mu_{\ln X}=\ln\left(\mu_X/\sqrt{1+\mathrm{COV}_X^2}\right), \tag{7}$$

$$\sigma_{\ln X}=\sqrt{\ln\left(1+\mathrm{COV}_X^2\right)}. \tag{8}$$

The value of the random field $F_X(x_i,y_i)$ at any position (x_i,y_i) in space is

$$F_X(x_i,y_i)=\exp\left[\mu_{\ln X}+\sigma_{\ln X}\cdot G(x_i,y_i)\right]. \tag{9}$$

2.2 Uncertainty in earthquake generation

Measured earthquake time history records exhibit inherent stochasticity and non-stationarity, which conventional simulation methods often inadequately represent (Z. Wang et al., 2024). This study employs an improved C–P spectrum (Deodatis, 1996) to generate more realistic non-stationary earthquake excitations. The bilateral power spectral density function for fully nonstationary excitation follows Cacciola and Deodatis (2011):

$$S_{\ddot{X}_{\mathrm{g}}}=A^2(t)\times\left[\frac{\omega^4}{\left[\omega^2-\omega_{\mathrm{f}}^2(t)\right]^2+4\xi_{\mathrm{f}}^2\omega_{\mathrm{f}}^2(t)\omega^2}\right]\times\left[\frac{\omega_{\mathrm{g}}^2(t)+4\xi_{\mathrm{g}}^2\omega_{\mathrm{f}}^2(t)\omega^2}{\left[\omega^2-\omega_{\mathrm{g}}^2(t)\right]^2+4\xi_{\mathrm{g}}^2\omega_{\mathrm{f}}^2(t)\omega^2}\right]\times S_0(t). \tag{10}$$

The parameters of the evolved power spectrum are shown in Eqs. (11)–(16) (Pang et al., 2021):

$$A(t)=\left[\frac{t}{c}\exp\left(1-\frac{t}{c}\right)\right]^d, \tag{11}$$

$$\omega_{\mathrm{g}}(t)=\omega_0-a\frac{t}{T}, \tag{12}$$

$$\xi_{\mathrm{g}}(t)=\xi_0+b\frac{t}{T}, \tag{13}$$

$$\omega_{\mathrm{f}}(t)=0.1\omega_{\mathrm{g}}(t), \tag{14}$$

$$\xi_{\mathrm{f}}(t)=\xi_{\mathrm{g}}(t), \tag{15}$$

$$S_0(t)=\frac{a_{\max}^2}{\gamma^2\pi\,\omega_{\mathrm{g}}(t)\left[2\xi_{\mathrm{g}}(t)+1/\xi_{\mathrm{g}}(t)\right]}, \tag{16}$$

where $A(t)$ is the time modulation function, c represents the occurrence time of peak acceleration, d is the shape control parameter, $a_{\max}$ is the peak acceleration of the earthquake excitation, T represents the duration of the earthquake excitation, ω_0 and ξ_0 are the initial circular frequency and equivalent damping ratio, respectively, which are determined by the site characteristics and the design earthquake grouping. Additional site-specific coefficients include a, b, and the equivalent crest factor γ.

The SR-random function method, which is shown in Eq. (17), provides a framework for characterizing this non-stationary excitation process, effectively capturing the temporal and spectral evolution of earthquake excitations. This approach enables the synthesis of realistic acceleration

time histories that properly account for both the frequency content variation and amplitude modulation observed in actual earthquake records.

$$\ddot{X}_g(t) = \sum_{K+1}^{N} \sqrt{2S_{\ddot{X}_g}(t,\omega_K)\Delta\omega}[\cos(\omega_K t)X_K + \sin(\omega_K t)Y_K], \tag{17}$$

where $\omega_K = K\Delta\omega$. The frequency separation must be small enough to meet the accuracy criteria. The upper cut-off frequency is set equal to 240 rad/s, while the $\Delta\omega$ is set equal to 0.15 rad/s. X_K, Y_K are the standard orthogonal random variables that satisfy the following conditions:

$$E[X_K] = E[Y_K] = E[X_K Y_K] = 0, \tag{18}$$

$$E[X_j X_K] = E[Y_j Y_K] = \delta_{jK}, \tag{19}$$

where $E[\cdot]$ represents the mathematical expectation and δ_{jK} is the Kronecker function. In the stochastic process, X_K and Y_K can be set to be functions of the basic random variable Θ:

$$X_K = \sqrt{2}\cos(K\Theta + \pi/4), \tag{20}$$

$$Y_K = \sqrt{2}\sin(K\Theta + \pi/4), K = 1, 2, \cdots, N, \tag{21}$$

where Θ is a random variable uniformly distributed on $[0, 2\pi]$. By constructing X_K and Y_K in this way, the requirements of Eqs. (18)–(19) can be satisfied.

To ensure compliance with seismic design codes, the generated acceleration time histories must satisfy the desired response spectrum. The average response spectrum ($S_{AR}(\omega, \zeta)$) of simulated earthquake excitations typically exhibits deviations from the target design spectrum ($S_{TD}(\omega, \zeta)$). These discrepancies are quantified using two key error metrics: the mean relative error ($\varepsilon_m < 5\%$) and maximum relative error ($\varepsilon_{max} < 10\%$). When these tolerance thresholds are exceeded, spectral modification becomes necessary to achieve code-compliant seismic inputs.

$$\varepsilon_m = \frac{1}{N}\sum_{K=1}^{N_f}\left|\frac{S_{TD}(T_K,\zeta) - S_{AR}(T_K,\zeta)}{S_{TD}(T_K,\zeta)}\right|, \tag{22}$$

$$\varepsilon_{max} = \max\left|\frac{S_{TD}(T_K,\zeta) - S_{AR}(T_K,\zeta)}{S_{TD}(T_K,\zeta)}\right|, \tag{23}$$

where ζ is the structural damping ratio, typically 0.05, T_K is the K-th discrete point of the response spectrum, and N_f is the total number of discrete points. When ε_m and ε_{max} cannot be satisfied, $S_{\ddot{X}_g}$ needs to be corrected according to Eq. (24):

$$S_{\ddot{X}_g}(t,\omega)_{m+1} = \begin{cases} S_{\ddot{X}_g}(t,\omega), & 0 < \omega \le \omega_c \\ S_{\ddot{X}_g}(t,\omega)_m \frac{S_{TD}(\omega,\zeta)^2}{S_{AR}(\omega,\zeta)^2}, & \omega > \omega_c \end{cases}, \tag{24}$$

where $S_{\ddot{X}_g}(t,\omega)_{m+1}$ and $S_{\ddot{X}_g}(t,\omega)_m$ represent the evolved power spectra after the m-th and $(m+1)$-th iterations, respectively. ω_c is the cutoff frequency, which is taken as 1.5 rad/s.

2.3 Performance function of tunnel lining system

Modern tunnel design primarily utilizes limit state approaches. This approach encompasses both serviceability limit states, controlling functional requirements like crack width and deformation, and ultimate limit states (ULS), ensuring structural integrity under extreme loading (Kroetz et al., 2018). This study concentrates specifically on ULS performance, as tunnel structures in seismic regions are typically governed by ultimate capacity considerations rather than serviceability requirements. The failure mechanism is characterized by three limit state functions (LSF) (Eqs. (25)–(27)) evaluating bending moment (M), axial force (N), and shear force (V) capacities (Guo et al., 2019). Structural failure occurs when any force component exceeds its capacity, mathematically indicated by a negative LSF value. LSFs account for each force component's distinct behavior: N uses a single limit state function because it is a completely positive value, while M and V are evaluated using absolute values to consider their sign-reversing characteristics. This approach addresses all critical loading scenarios that may occur during seismic excitation.

$$LSF_M = M_{limit} - |M|_{max}, \tag{25}$$

$$LSF_N = N_{limit} - N_{max}, \tag{26}$$

$$LSF_V = V_{limit} - |V|_{max}, \tag{27}$$

where M_{limit}, N_{limit}, and V_{limit} are the limit states of M, N, and V, respectively. This study employs deterministic limit state capacities (M_{limit}, N_{limit}, V_{limit}) in the analysis, as their inherent uncertainties are negligible compared to the substantial spatial variability of rock mass properties (Kroetz et al., 2018).

2.4 Reliability analysis using MCS

This study conducts a reliability analysis of tunnel linings under earthquake action, considering the uncertainty of rock mass properties and earthquake excitations using MCS. The probability of failure (P_f) is determined through repeated random analyses with randomized input parameters (rock mass properties and earthquake excitations), where failure occurrences are counted when the response exceeds LSFs (Guo et al., 2019). The simulation employs a convergence criterion based on the coefficient of variation of P_f ($COV_{Pf} \le 5\%$), ensuring statistical reliability of results. This threshold determines the required number of MCS realizations (N_{MCS}), balancing computational efficiency with result accuracy.

$$COV_{Pf} = \sqrt{\frac{1 - P_f}{N_{MCS} \cdot P_f}}. \tag{28}$$

During reliability analysis with MCS, P_f was obtained using the following equations:

$$P_f = \frac{1}{N_{MCS}} \sum_{n=1}^{N_{MCS}} I, \tag{29}$$

$$I = \begin{cases} 0 & \text{if} \quad \mathrm{LSF}_M, \mathrm{LSF}_N, \mathrm{LSF}_V > 0, \\ 1 & \text{else}, \end{cases} \tag{30}$$

where I is an indicator function. The I of a failure case is a random variable that takes a value of 1 when any of the LSFs is negative, meaning that the structure has failed, and a value of 0 when the LSFs are all positive. Although computationally demanding, MCS is employed in this study due to its robustness and ability to handle complex reliability problems involving multiple failure modes and coupled uncertainties (rock properties and earthquake excitations).

2.5 Implementation procedure

Figure 1 illustrates the schematic workflow of this study, consisting of six key steps, summarized as follows:

Step 1: Determine statistical parameters, including tunnel dimensions, concrete properties, and the mean of rock properties, based on engineering data and laboratory tests. A tunnel model was developed using the finite element method (FEM) and ABAQUS software.

Step 2: Determine the parameters of random fields and C–P power spectrum.

Step 3: Generate N_{MCS} sets of random fields using K–L expansion methods described in Section 2.1 and N_{MCS} sets of random earthquake excitations using the method described in Section 2.2.

Step 4: Replace the rock mass parameter values in the original tunnel model with those derived from the random fields. Also, the original earthquake excitation needs to be replaced by random earthquake excitations.

Step 5: Compute the N_{MCS} sets of random models and extract the corresponding results.

Step 6: Perform a statistical analysis of the results for the assessment of the tunnel's dynamic response.

3 Case study

3.1 General description

This study investigates the T-Tunnel on a railway route (Fig. 2), located in a region characterized by pronounced north–south topographic gradients and significant terrain undulations. The tunnel alignment traverses elevations between 2135 and 3775 m, encompassing relative elevation differences of 1100 to 1500 m.

In compliance with Seismic Ground Motion Parameters Zonation Map of China (Institute of Geophysics, China Earthquake Administration et al., 2015), the T-Tunnel site is characterized by a design peak ground acceleration of

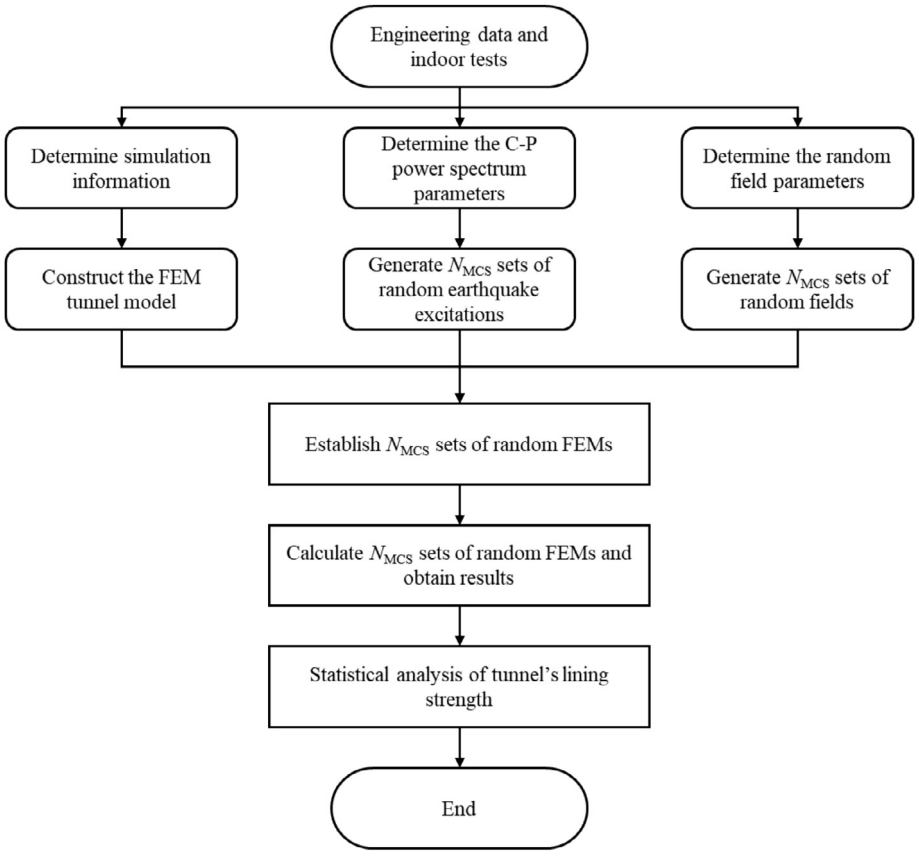

Fig. 1. Flowchart of the framework of this research.

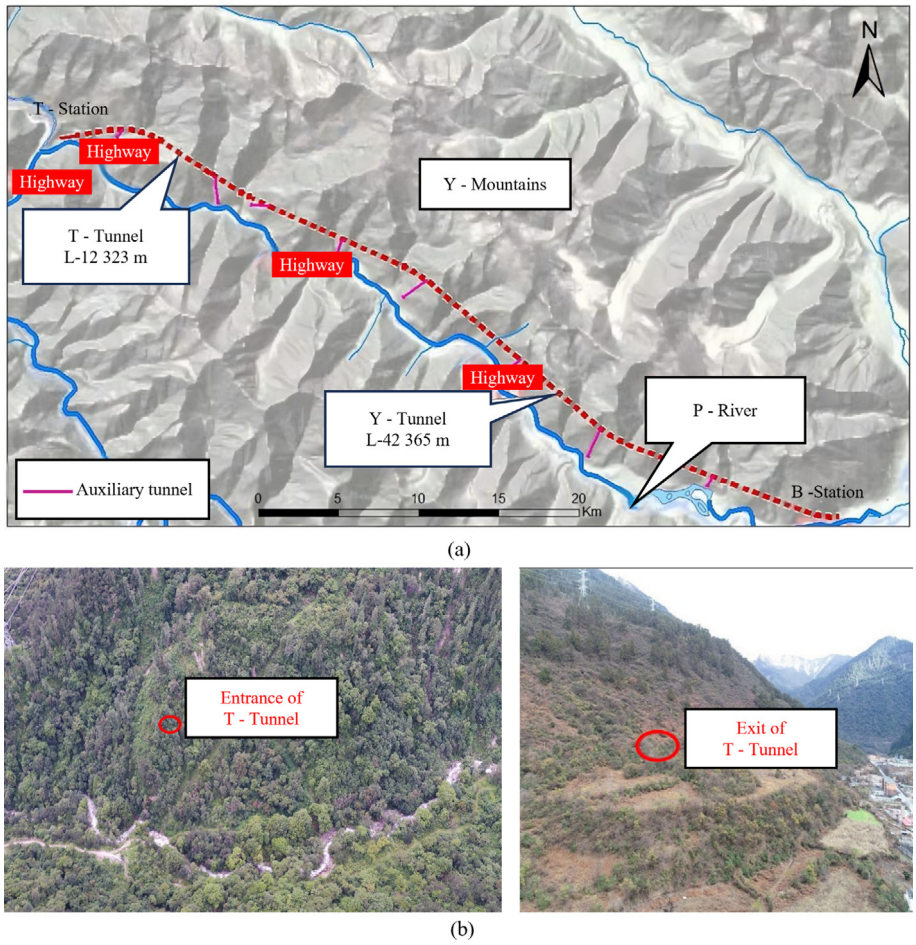

Fig. 2. Location of the study area. (a) T-Tunnel topography diagram, and (b) entrance and exit of the T-Tunnel.

0.20*g* for Class II site conditions, corresponding to an exceedance probability of 10% in 50 years and equivalent to a seismic intensity of VIII on the Chinese scale. The comprehensive geotechnical investigation program included 70 boreholes totaling 12 323.4 m of drilling, with detailed core logging and documentation of 185 retrieved samples. These cores underwent extensive laboratory testing, including 1380 uniaxial compression tests, 245 direct shear tests, and 239 triaxial compression tests, to determine the mechanical parameters of the rock mass. This rigorous experimental program provides the essential foundation for the subsequent seismic performance evaluation of the tunnel.

3.2 Constitutive model and calculation parameters

A simplified two-dimensional finite element model was established using ABAQUS to evaluate the seismic performance of the tunnel lining structure (Fig. 3). The model dimensions measure 200 m in both length and height, with 5 m wide infinite element boundaries implemented to eliminate wave reflection effects. The tunnel profile consists of a 12 m diameter circular cross-section with a 0.4 m thick C30 concrete lining according to GB 50010—2010 (Ministry of Housing and Urban-Rural Development of the People's Republic of China, 2010), positioned 94 m below the upper boundary. The numerical model utilizes 20 520 quadrilateral elements (20 871 nodes) with a uniform maximum size of 1.5 m in both horizontal and vertical directions. This mesh configuration satisfies two critical criteria: (1) the 1/8–1/10 wavelength associated with the highest frequency component for peak velocities through the medium (Kuhlemeyer & Lysmer, 1973), and (2) the spatial discretization condition (element size $<$ 0.13SOF–0.17SOF) necessary for proper representation of geotechnical parameter variability in random field analysis (Ching & Phoon, 2013b). The dual compliance ensures simultaneous accuracy in both dynamic response computation and spatial uncertainty characterization. The interface between the surrounding rock and the lining was simulated using a combined Lagrange multiplier-penalty approach, with the concrete lining as the master surface and the surrounding rock as the slave. Normal behavior follows Hooke's law, while tangential response is governed by Coulomb friction with a coefficient of 0.5. Boundary conditions consisted of (1) fixed base with horizontally constrained sides for static equilibrium analysis under gravitational loading, and (2) bidirectional seismic input (vertical acceleration = 2/3

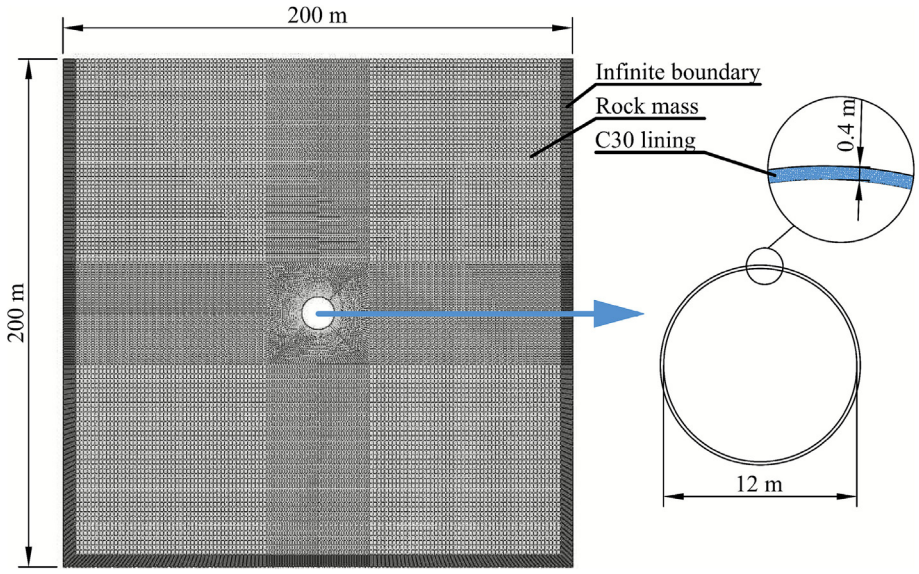

Fig. 3. Numerical model.

Table 1
Calculation parameters of rock mass.

Parameter	Unit	Value
Density (ρ)	kg/m^3	2700
Elastic modulus (E)	GPa	3.50
Poisson's ratio (υ)	–	0.26
Cohesion (c)	kPa	650
Friction angle (φ)	°	35

Table 2
Random field parameters of random variables.

Parameter	μ_X	COV$_X$	SOF$_X$	
			δ_{hX}	δ_{vX}
ρ	2700 kg/m^3	3.20%	74.51 m	15.22 m
E	3.50 GPa	43.55%		

horizontal) for subsequent implicit dynamic time-history analysis. The two-stage computational procedure first established initial stress equilibrium, then performed seismic response analysis using these equilibrated stresses as initial conditions.

The rock mass is characterized using the Mohr–Coulomb model (Table 1). Simulating all material parameters as random fields would entail prohibitive computational costs. To overcome this challenge, a Sobol sensitivity analysis was conducted to identify the most influential parameters. As shown in Fig. 4, density (ρ) and elastic modulus (E) exhibit a substantial influence on the structural response, while the contribution of shear strength parameters—cohesion (c) and friction angle (φ)—is comparatively moderate.

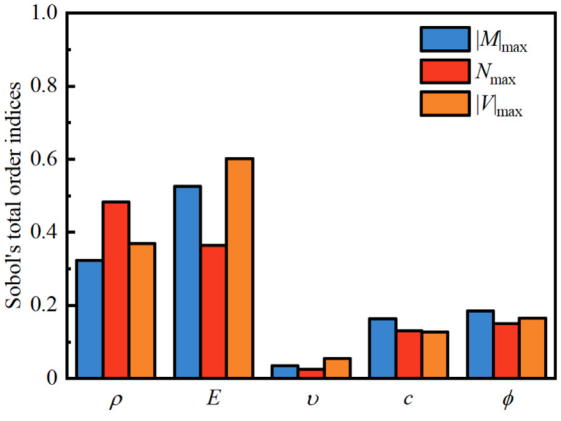

Fig. 4. Sobol's indices indicating the sensitivities of rock mass parameters.

The computational efficiency of models incorporating different stochastic parameter combinations was evaluated on an Intel i5-12600KF CPU. Simulations involving all five parameters (ρ, E, υ, c, φ) required approximately 2500 s. Omitting Poisson's ratio (i.e., considering only ρ, E, c, φ) reduced the computation time to 1800 s. By further restricting the stochastic parameters to only the highly sensitive ones—ρ and E—computational time was dramatically reduced to just 300 s per simulation. Each simulation covers the complete workflow, including stochastic parameter generation, model construction and parsing, numerical computation, and result extraction. This substantial improvement in computational efficiency-an 88% reduction compared to the full model-is critical to the feasibility of the MCS used in this study, significantly enhancing the practicality and viability of the proposed framework. Therefore, this study identifies ρ and E as the key random variables. Their statistical characteristics (μ_X and COV$_X$) were determined from laboratory test data, while their

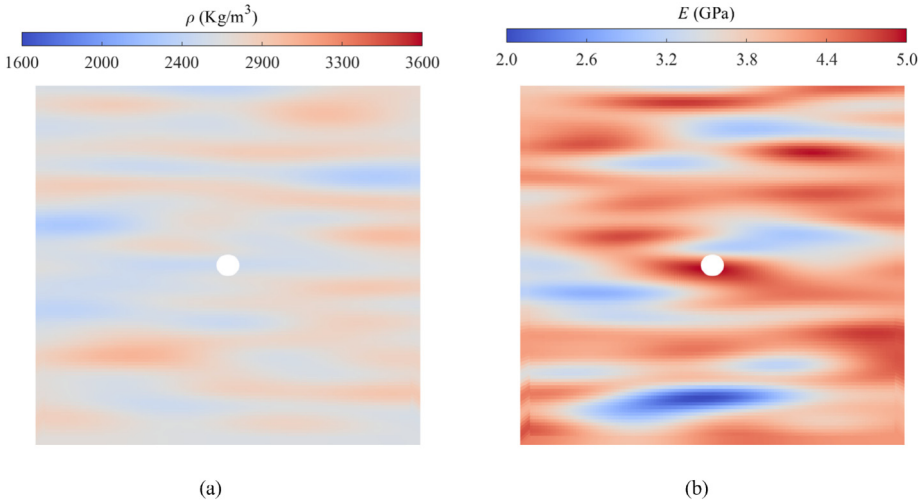

Fig. 5. Typical random field of rock mass properties. (a) ρ, and (b) E.

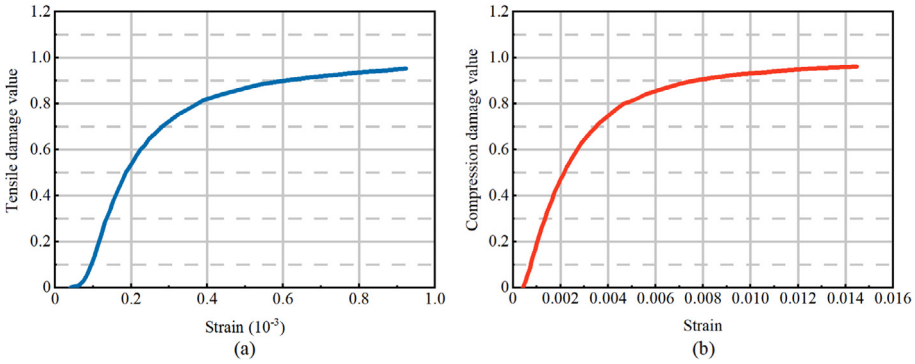

Fig. 6. Uniaxial tensile and compression damage evolution curves for C30. (a) Uniaxial tensile, and (b) uniaxial compression.

Table 3
Random earthquake excitation generation parameters.

T (s)	ω_0 (rad/s)	ξ_0	a (rad/s)	b	c (s)	d	γ	a_{max} (g)
10	19	0.55	4	0.25	4	2	2.6	0.2

SOF_X were derived through the MLE method in Section 2.1. The random field parameters of ρ and E were shown in Table 2.

It should be emphasized that this area is categorized as Class IV surrounding rock according to Code for Design of Railway Tunnel Design (China Railway Second Design Institute Engineering Group Co., Ltd, 2017). The geological conditions feature weakly weathered gneiss with extensively developed joint systems and fracture networks, leading to a highly fragmented rock mass structure with pronounced heterogeneity in mechanical properties. Consequently, COV_E obtained through comprehensive laboratory testing demonstrates relatively higher values compared to conventional rock masses, which is consistent with the expected behavior of such geologically complex formations.

Figure 5 illustrates the simulated spatial distributions of ρ and E for a typical numerical realization. The color bar ranges for ρ and E were set to $\mu_X \pm 0.333\mu_X$ to standardize dispersion visualization across models. E exhibits more pronounced variability than ρ due to its significantly higher coefficient of variation ($COV_E > COV_\rho$), reflecting their differing degrees of spatial heterogeneity in the rock mass properties.

The density of the C30 concrete is 2400 kg/m^3, the elastic modulus is 30 GPa, and Poisson's ratio is 0.2. The concrete damaged plasticity model, which was developed by Lee and Fenves (1998), is used for C30 concrete lining. Uniaxial tensile and compressive damage evolution curves for C30 (Fig. 6) can be obtained according to GB 50010—2010 (Ministry of Housing and Urban-Rural Development of the People's Republic of China, 2010).

The nonstationary random earthquake excitations were generated using the parameters listed in Table 3 combined with the theory in Section 2.2. The mean value and standard deviation time histories of generated random earthquake excitations are shown in Fig. 7(a) and (b). It is evident that the generated random earthquake excitation exhibits a high level of fitting effectiveness and can satisfy

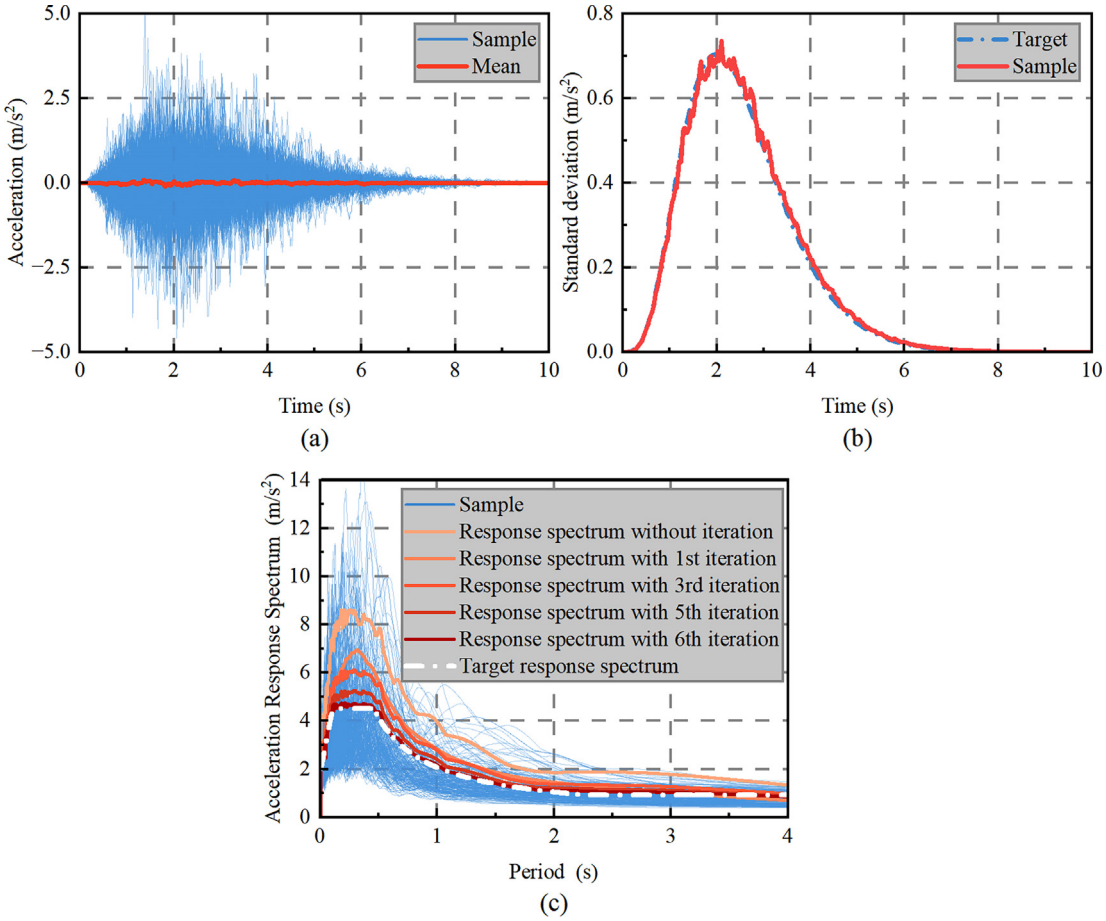

Fig. 7. Random earthquake excitations. (a) Samples and mean of earthquake excitations, (b) standard deviation of earthquake excitations, and (c) acceleration spectrum fitting curves.

Table 4
ε_m and ε_{max} for iterations.

Iteration time	ε_m (%)	ε_{max} (%)
0	80.63	94.28
1	37.31	53.81
3	29.67	36.89
5	5.88	11.30
6	2.81	8.09

the calculation requirements. The target response spectrum was established according to the Code for Seismic Design of Railway Engineering (Ministry of Railways of the People's Republic of China, 2006), with spectral matching achieved through iterative correction using Eq. (24). As demonstrated in Table 4, ε_m and ε_{max} progressively decreased with each iteration, achieving full compliance with seismic code requirements after six iterations. The corrected excitation time histories (Fig. 7(c)) show excellent agreement with the target spectrum across all frequency ranges. These results confirm that the generated random earthquake excitations not only satisfy regulatory requirements but also maintain proper nonstationary characteristics essential for accurate seismic response analysis.

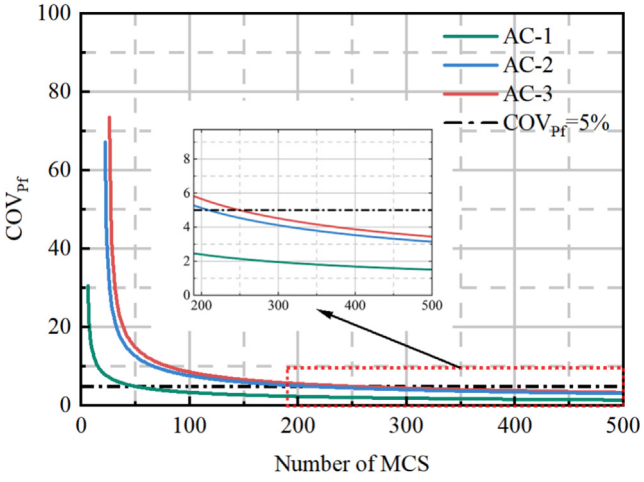

Fig. 8. Convergence analysis of MCS.

3.3 Analysis condition design

This study evaluates the reliability of tunnel lining under seismic loading through an analysis of three analysis conditions (AC), examining different combinations of

uncertainty sources. The analysis compares cases considering only variability of rock mass properties (AC-1), only randomness in earthquake excitation (AC-2), and both factors simultaneously (AC-3). A consistent finite element modeling framework is maintained across all cases to ensure comparable probability assessments, with AC-1 and AC-3′s rock mass properties using the random fields with parameters shown in Table 2, while the AC-2 employs determined rock mass properties (Table 1). For the earthquake excitation, the response spectrum of AC-1′s determined earthquake excitation is consistent with the target response spectrum. The random earthquake excitations for AC-2 and AC-3 were generated based on the parameters shown in Table 3.

Structural reliability is quantified through P_f analysis using experimentally validated limit state criteria for 0.4 m thick C30 lining: M_{limit} is 0.5 MN·m, N_{limit} is 8.2 MN, and V_{limit} is 0.75 MN (Guo et al., 2019; Kroetz et al., 2018). The MCS framework employs 500 iterations per analysis case, determined through convergence testing where the COV_{Pf} falls below the 5% threshold (Fig. 8). This approach provides statistically reliable results while maintaining computational efficiency for the evaluation of multiple failure modes under different uncertainty combinations.

3.4 Result analysis

3.4.1 Mechanical behavior of lining

Figure 9 presents the probability density functions (PDFs) and cumulative distribution functions (CDFs) of $|M|_{max}$, N_{max}, and $|V|_{max}$ under different ACs. The results demonstrate distinct distribution patterns across the considered uncertainty scenarios. When both random factors are considered simultaneously, the mean values of structural responses show significant increases compared to single-factor cases. Specifically, the AC-3 yields a mean $|M|_{max}$ of 0.137 MN·m, representing a 251.3% increase over the AC-1 (0.039 MN·m) and a 9.6% increase over the AC-2 (0.125 MN·m). Similarly, the mean N_{max} under AC-3 reaches 0.91 MN, exceeding the AC-1 by 107.8% and the AC-2 by 9.6%. The most pronounced difference appears in $|V|_{max}$, where the AC-3 mean of 0.072 MN surpasses the AC-1 result by 278.9% and the AC-2 result by 24.1%.

Table 5 presents the statistical characteristics of tunnel mechanical behavior of lining under different ACs, revealing that the COV under AC-3 shows a significant increase compared to AC-1. Specifically, the COV increases by 30.1% for $|M|_{max}$, 194.2% for N_{max}, and 262.8% for $|V|_{max}$. When compared to AC-2, AC-3′s COV remains slightly higher with increases of 4.87%, 16.3%, and 19.3%

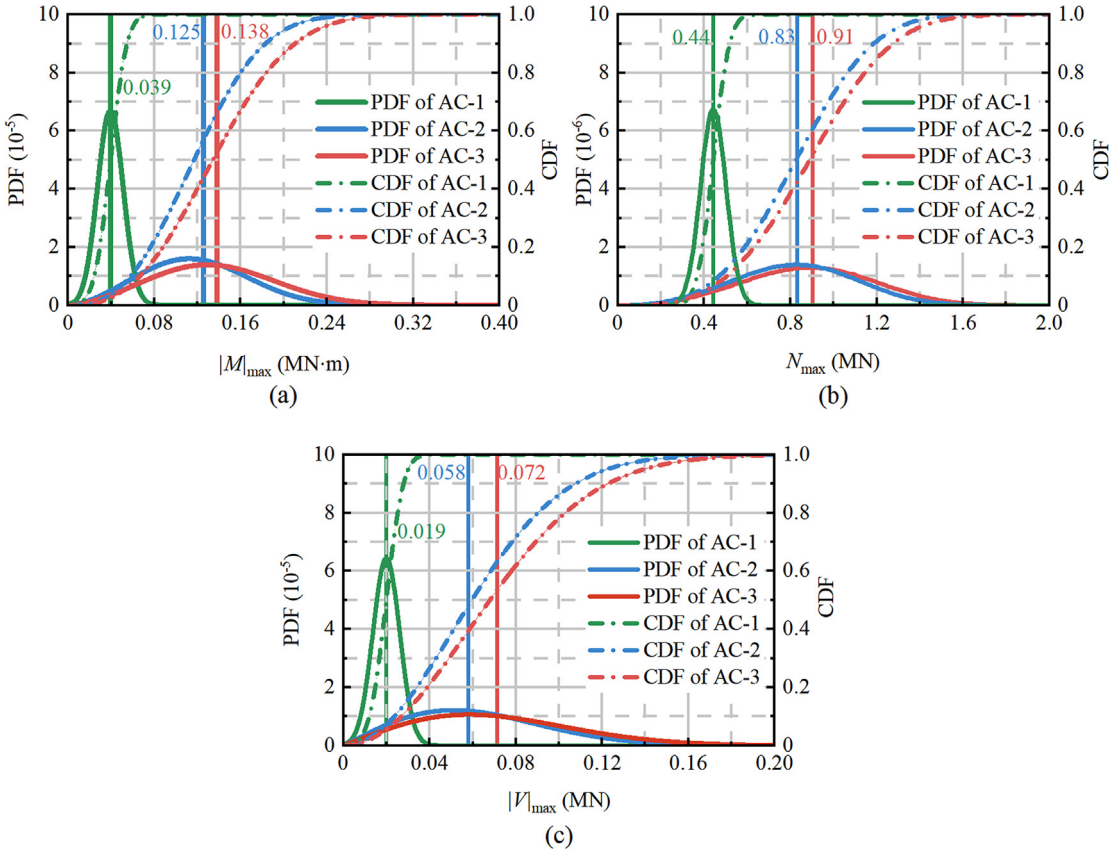

Fig. 9. PDFs and CDFs for the mechanical behavior of lining. (a) PDFs and CDFs of $|M|_{max}$, (b) PDFs and CDFs of N_{max}, and (c) PDFs and CDFs of $|V|_{max}$.

Table 5
Statistical table of mechanical behavior of lining under different ACs.

Analysis condition	Mechanical behavior of lining	Mean	Coefficient of variation (%)	*P*-value
AC-1	$\|M\|_{max}$	0.039	30.2	0.12
	N_{max}	0.44	10.4	0.14
	$\|V\|_{max}$	0.019	31.2	0.09
AC-2	$\|M\|_{max}$	0.13	37.5	<0.05
	N_{max}	0.83	26.3	<0.05
	$\|V\|_{max}$	0.058	94.9	<0.05
AC-3	$\|M\|_{max}$	0.137	39.3	<0.05
	N_{max}	0.91	30.6	<0.05
	$\|V\|_{max}$	0.073	113.2	<0.05

for $|M|_{max}$, N_{max}, and $|V|_{max}$, respectively. These results demonstrate that the combined effect of both random factors leads to greater dispersion in the mechanical behavior of lining response than either factor considered individually. The particularly substantial increases relative to AC-1 highlight how seismic randomness dominates the response variability, while the more modest differences from AC-2 indicate that incorporating rock mass properties' variability introduces additional, though secondary, uncertainty effects. This amplification of response dispersion underscores the importance of considering both uncertainty sources simultaneously for reliable seismic performance assessment. The Anderson-Darling normality tests yield *P*-values below the 0.05 significance threshold for all results of AC-2 and AC-3, rejecting the normal distribution hypothesis, a finding that contrasts with results from AC-1. This fundamental shift in statistical behavior, induced by seismic uncertainty, indicates that earthquake randomness not only increases response magnitudes but also introduces greater complexity in the underlying probability distributions. The resultant response patterns become more difficult to characterize and predict compared to cases considering only rock mass properties' variability.

Figure 10 demonstrates the temporal evolution of probability density distributions for $|M|$, N, and $|V|$ during the 1–10 s seismic excitation period, revealing distinct dynamic response characteristics under different uncertainty conditions. The probability density functions exhibit pronounced temporal variations that deviate significantly from conventional normal or lognormal distribution assumptions. Analysis of the evolving distributions shows that AC-1 produces relatively concentrated response patterns, while AC-2 and AC-3 display substantially greater dispersion, particularly during the 1.5–5 s interval when seismic energy is most intense. The slightly broader distributions observed in AC-3 compared to AC-2 confirm the additional, though secondary, influence of material variability on response dispersion. The results collectively demonstrate that while seismic randomness dominates the overall response variability, the combined effect of both uncertainty sources produces unique distribution characteristics that cannot be captured through single factor analyses or conventional distribution assumptions. This underscores the necessity of employing analysis approaches that simultaneously account for both rock mass properties and loading uncertainties during analysis of the seismic performance of tunnel lining.

The results demonstrate that considering only single uncertainty sources, particularly just rock mass properties' spatial variability, substantially underestimates the mechanical behavior of lining and produces conservative safety estimates. While earthquake excitation dominates structural response (evidenced by similar AC-2 and AC-3), rock mass properties' spatial variability introduces additional dispersion that cannot be neglected. The non-normal distributions and amplified responses under dual uncertainties reveal complex interaction effects, necessitating advanced probabilistic methods that simultaneously account for both the uncertainty of rock mass properties and earthquake excitations in tunnel seismic design. This approach is crucial for reliable performance assessment, as conventional single-factor analyses may significantly compromise prediction accuracy and structural safety.

3.4.2 Probability of failure

Figure 11 presents the probability distributions of the limit state functions, clearly showing that M dominates the failure probability of tunnel linings, with its LSF_M distributions located closest to the failure threshold ($LSF < 0$). V exhibits intermediate failure probability, while N demonstrates the highest safety margin as evidenced by LSF_N values remaining farthest from the failure domain. The results quantitatively demonstrate that structural safety is primarily controlled by flexural capacity, with substantially lower probabilities of failure in shear and especially axial modes.

Table 6 presents a quantitative reliability assessment of tunnel lining performance under different uncertainty conditions. The results demonstrate a clear hierarchy in failure probabilities across limit states: M shows the highest values (AC-1: 0%, AC-2: 1.4%, AC-3: 1.8%), followed by V and N, establishing a consistent $M > V > N$ vulnerability ranking. This pattern indicates that LSF_N and LSF_V contribute minimally to system failure probability under the examined

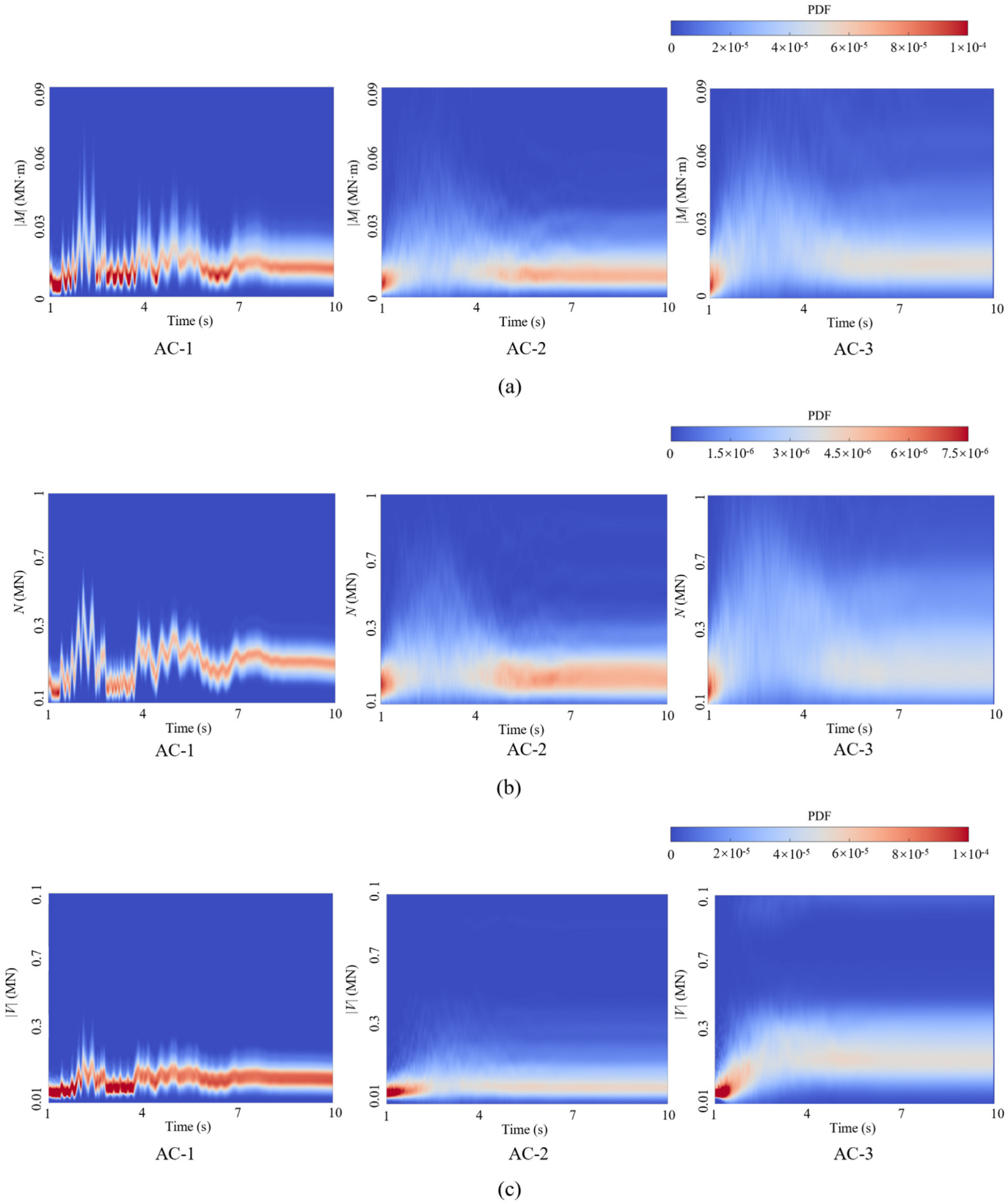

Fig. 10. Temporal evolution of PDFs for the mechanical behavior of lining. (a) $|M|$ of different ACs, (b) N of different ACs, and (c) $|V|$ of different ACs.

conditions. The system reliability analysis shows that AC-3 yields significantly higher (more conservative) failure probabilities than AC-1 and moderately higher values than AC-2, with system failure probabilities of 0%, 1.4%, and 1.9% for AC-1, AC-2, and AC-3, respectively. These results provide numerical validation that seismic design must

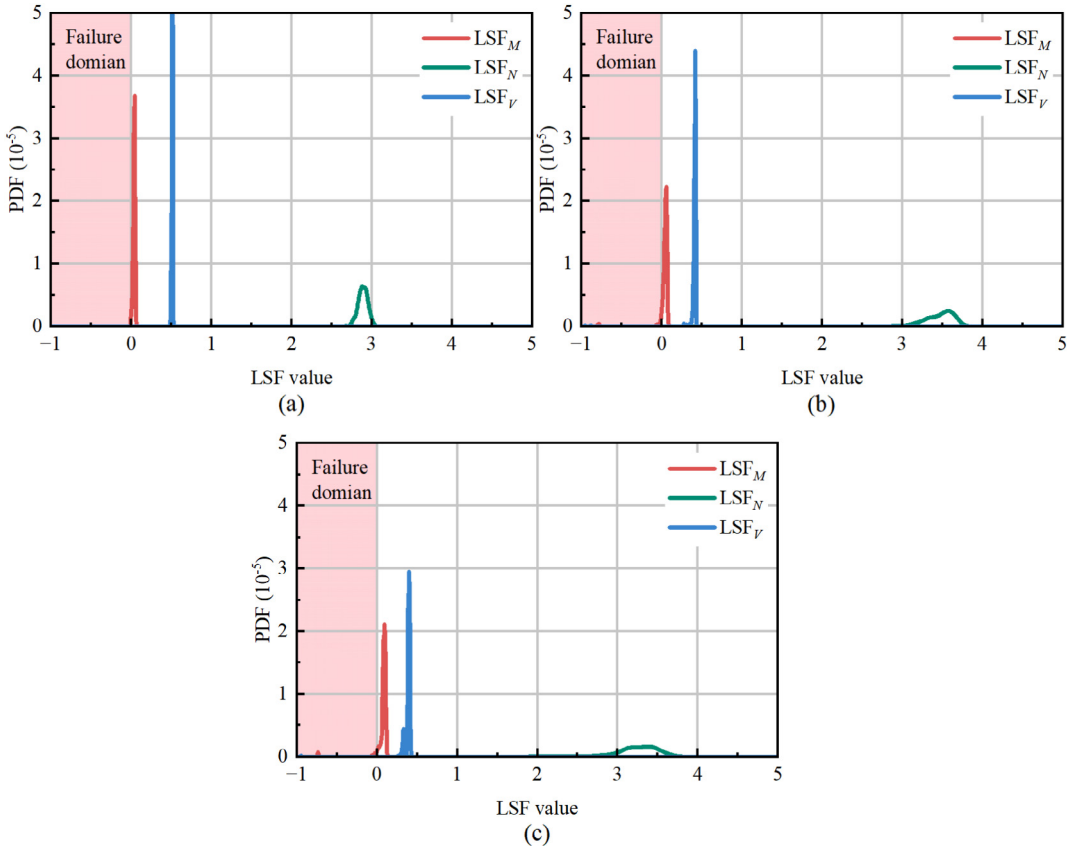

Fig. 11. Value of LSFs. (a) AC-1, (b) AC-2, and (c) AC-3.

Table 6
Reliability results of lining structure.

Analysis condition	LSF	Probability of failure (%)
AC-1	LSF$_M$	0
	LSF$_N$	0
	LSF$_V$	0
	System	0
AC-2	LSF$_M$	1.4
	LSF$_N$	0
	LSF$_V$	0
	System	1.4
AC-3	LSF$_M$	1.8
	LSF$_N$	0.2
	LSF$_V$	0.2
	System	1.9

simultaneously account for both material and loading uncertainties to achieve adequate safety margins, as considering either factor alone leads to conservative reliability estimates, particularly when neglecting the uncertainty of earthquake excitation.

4 Parametric study

This study's findings, while demonstrating the critical need to consider both earthquake excitation and geotechnical uncertainties in tunnel design, involve several important assumptions that merit discussion. The analysis employed an improved C–P spectrum model whose key parameters, initial circular frequency (ω_0) and equivalent damping ratio (ξ_0), introduce additional uncertainty due to the absence of standardized estimation methods. As noted by Marano et al. (2008), the selection of these spectral parameters can significantly influence structural response predictions, a fundamental challenge inherent to numerical simulation approaches. To systematically address these issues, this study performed a detailed parametric analysis to evaluate the influence of variations in both ω_0 and ξ_0. The selected ranges for ω_0 (10–50 rad/s) and ξ_0 (0.1–0.9) were adopted based on values reported in Xu et al. (2025) and Luo and Peng (2024). In addition, the differences in response between AC-3 and AC-1/2 under varying peak ground acceleration conditions (a_{max} = 0.2g–1.2g) are discussed. The effect of the variation of a_{max} on P_f of the tunnel lining structure is also discussed.

4.1 Effect on initial circular frequency

ω_0 serves as a fundamental parameter in earthquake excitation characterization, significantly impacting the dynamic response of tunnel structures. A parametric investigation was conducted by varying ω_0 across five discrete values (10–50 rad/s) to systematically evaluate its effect

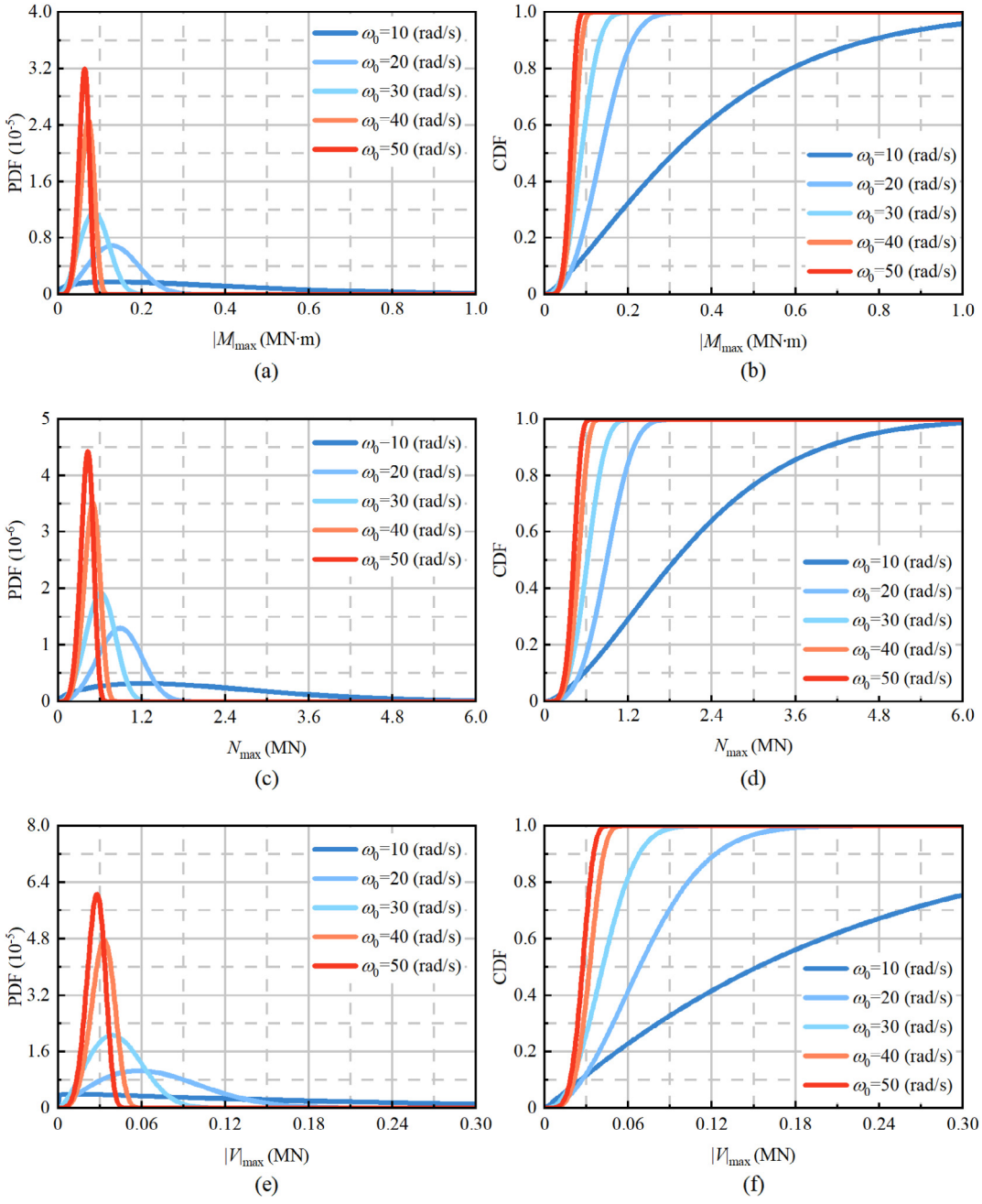

Fig. 12. PDFs and CDFs of the mechanical behavior of lining under different ω_0. (a) PDFs of $|M|_{max}$, (b) CDFs of $|M|_{max}$, (c) PDFs of N_{max}, (d) CDFs of N_{max}, (e) PDFs of $|V|_{max}$, and (f) CDFs of $|V|_{max}$.

on tunnel lining performance. Figure 12 shows PDFs and CDFs of the mechanical behavior of lining. The analysis reveals a substantial reduction in both the mean values and dispersion of structural responses: $|M|_{max}$ decreases from 0.37 to 0.061 MN·m (83.5% reduction) with a corresponding decrease in COV from 87.8% to 17.7% (79.8% reduction). Similarly, N_{max} shows a reduction from 2.1 to 0.51 MN (75.7% decrease) with COV decreasing from 71.6% to 18.5% (74.2% reduction), while $|V|_{max}$ demonstrates an 87.2% reduction (0.211 to 0.027 MN) accompanied by COV decrease from 121.1% to 21.2% (82.5% reduction). These findings indicate that higher ω_0 values produce more conservative estimates of lining demands. Consequently, for enhanced structural safety, seismic design of tunnels should preferentially consider the lowest value of the range of site-specific ω_0 values when characterizing design earthquake excitations, further emphasizing the importance of proper spectral parameter selection in tunnel seismic design.

4.2 Effect on equivalent damping ratio

ξ_0 represents another critical site-specific parameter that significantly influences earthquake excitation

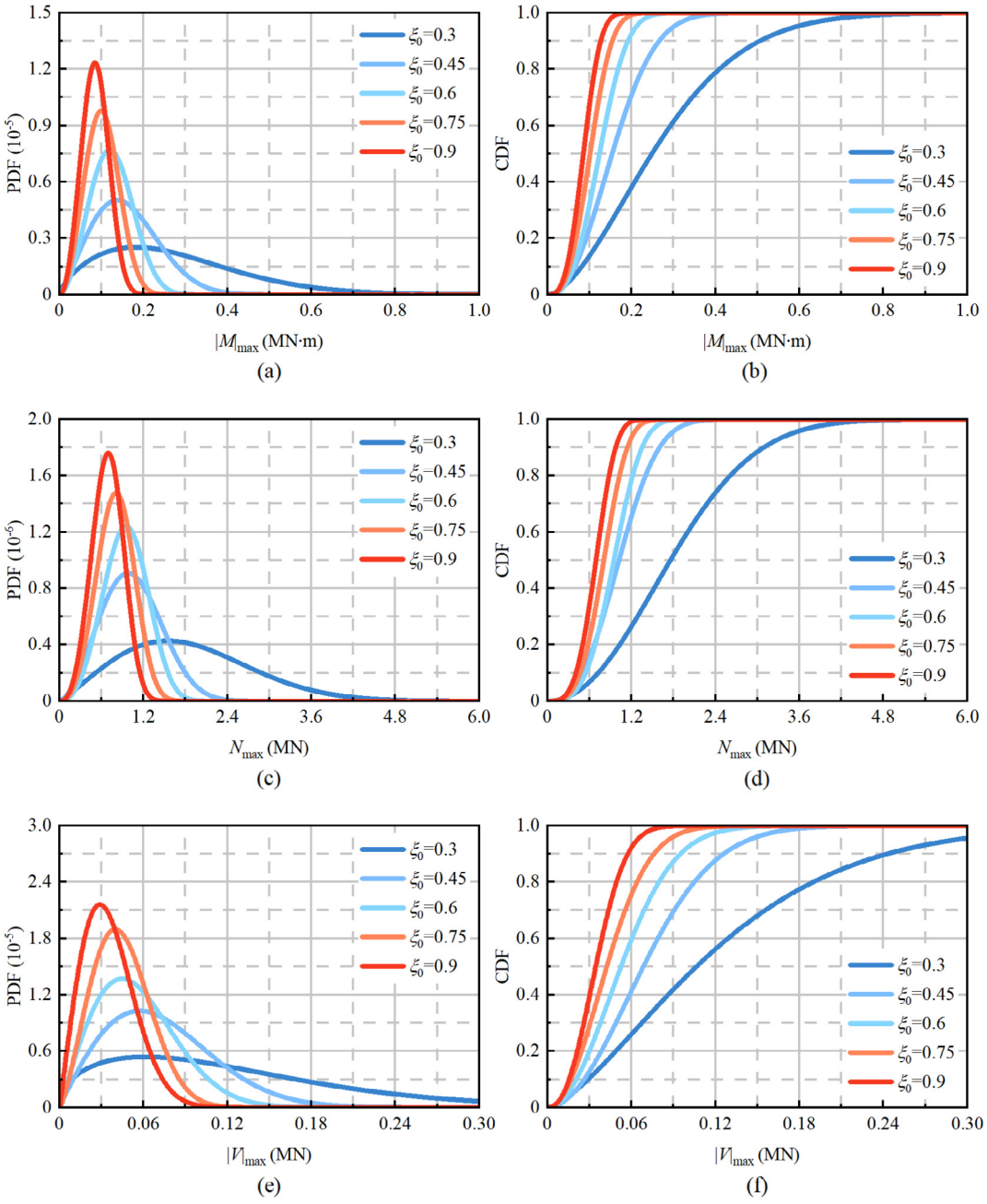

Fig. 13. PDFs and CDFs of the mechanical behavior of lining under different ξ_0. (a) PDFs of $|M|_{max}$, (b) CDFs of $|M|_{max}$, (c) PDFs of N_{max}, (d) CDFs of N_{max}, (e) PDFs of $|V|_{max}$, and (f) CDFs of $|V|_{max}$.

characteristics and tunnel structural response. Through systematic variation of ξ_0 from 0.3 to 0.9, Fig. 13 shows PDFs and CDFs of the mechanical behavior of the lining. Mean of $|M|_{max}$ decreases by 67.5% (from 0.27 to 0.0877 MN m) while its COV drops from 66.8% to 31.3% (53.1% reduction) with increasing ξ_0. Similar trends are observed for N_{max}, 62.9% reduction of its mean from 0.17 to 0.063 MN with COV decreasing from 49.7% to 27.1% (45.5% reduction) and $|V|_{max}$, 70% reduction of its mean from 0.12 to 0.036 MN with COV decreasing from 84.8% to 42.4% (50% reduction). While the sensitivity of structural response to ξ_0 variation is less pronounced compared to ω_0 effects, the observed changes remain substantial, particularly within the ξ_0 range of 0.30–0.45, where the most significant response variations occur. Consequently, seismic design of tunnels should carefully consider the lowest value of the range for site-specific ξ_0 to ensure adequate safety margins.

4.3 Effect on peak acceleration

a_{max} plays a pivotal role in seismic analysis by directly determining the intensity of earthquake excitation and significantly influencing structural performance assessments. This study examines a_{max} values ranging from 0.2g to 1.2g to evaluate their effects on tunnel lining response

characteristics. As shown in Fig. 14, the PDFs and CDFs of $|M|_{max}$, N_{max}, and $|V|_{max}$ exhibit distinct patterns under varying a_{max} levels. The analysis reveals that increasing a_{max} causes a systematic rightward shift in the PDFs of all three force components, reflecting a higher mean value under stronger earthquake excitations. For $|M|_{max}$ and N_{max}, the PDFs initially broaden between $0.2g$ and $0.4g$ before becoming more concentrated at higher acceleration levels, while their CDFs transition from relatively flat to steeper profiles. This behavior results from the combined effects of expanding response ranges and the increasing dominance of a_{max} over other parameters at higher intensities. The distribution patterns of $|M|_{max}$ and N_{max} evolve characteristically with increasing a_{max} due to their positive-definite nature. At low a_{max} ($0.2g$), responses remain small and concentrated, producing asymmetric distributions. As a_{max} rises to $0.4g$, the expanding response range leads to broader with increased dispersion. However, beyond $0.4g$, two effects dominate: (1) a_{max} becomes the primary response determinant, diminishing other parameters' influence, and (2) approaching structural limits constrains response dispersion. These mechanisms cause dispersion to peak around $0.4g$ before decreasing at higher intensities, despite continued growth in mean response

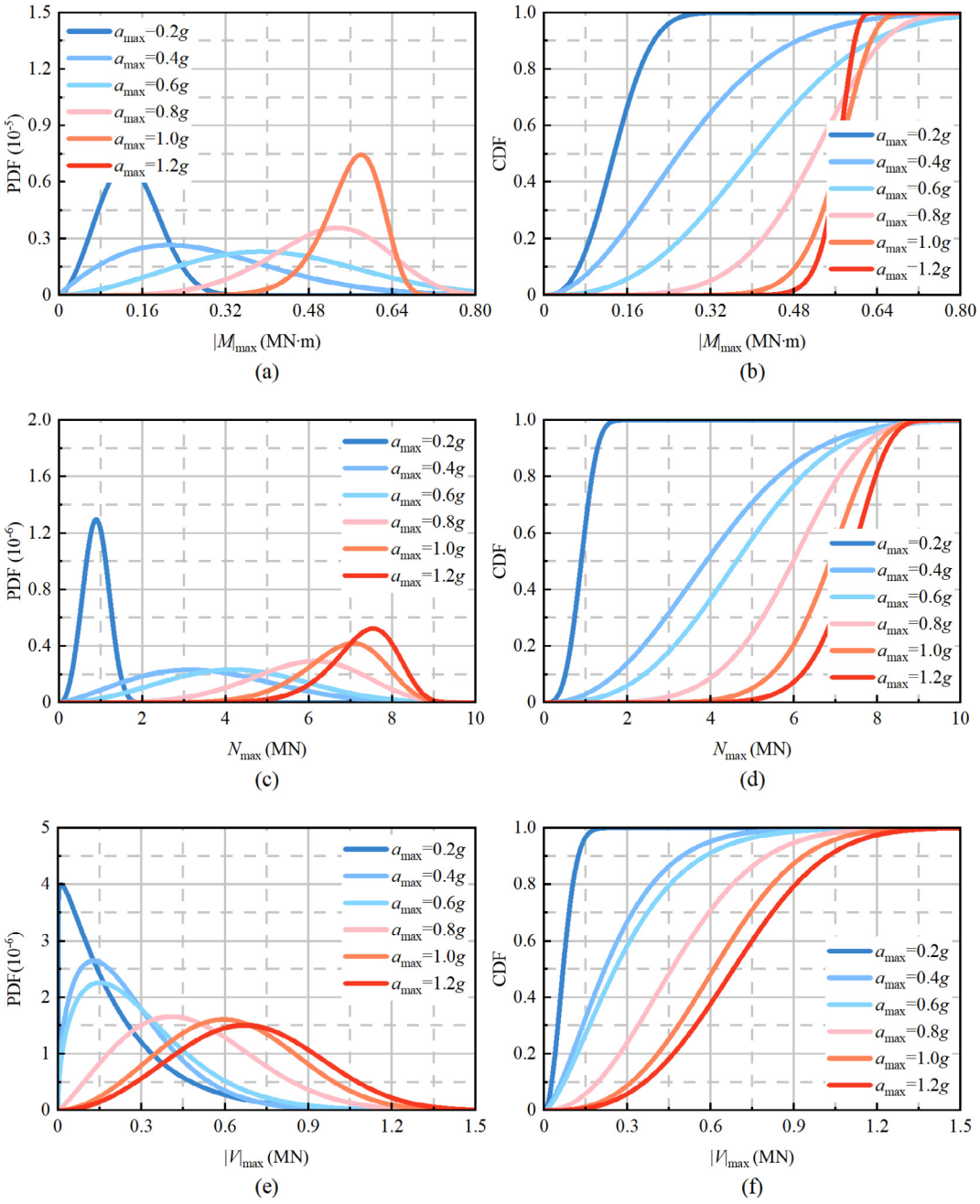

Fig. 14. PDFs and CDFs of the mechanical behavior of lining under different a_{max}. (a) PDFs of $|M|_{max}$, (b) CDFs of $|M|_{max}$, (c) PDFs of N_{max}, (d) CDFs of N_{max}, (e) PDFs of $|V|_{max}$, and (f) CDFs of $|V|_{max}$.

values. $|V|_{max}$ demonstrates different distribution characteristics, with its PDF progressively flattening and CDF becoming more horizontal as a_{max} increases.

Figure 15 depicts the mean and COV of $|M|_{max}$, N_{max}, and $|V|_{max}$ as a_{max} increases under different ACs. For $|M|_{max}$, AC-2 and AC-3 show similar patterns in both mean values and COV trends. At $a_{max} = 0.2g$, the means of $|M|_{max}$ are 0.039 MN·m (AC-1), 0.12 MN·m (AC-2), and 0.14 MN·m (AC-3), with AC-3 representing increases of 2.5 and 0.1 times over AC-1 and AC-2, respectively. This difference amplifies substantially at $a_{max} = 1.2g$, where means reach 0.125 MN·m (AC-1), 0.487 MN·m (AC-2), and 0.560 MN·m (AC-3), corresponding to 4.5 and 1.1 times increases for AC-3. For N_{max}, AC-2, and AC-3 again demonstrate parallel trends. At $a_{max} = 0.2g$, mean values of N_{max} are 0.44 MN (AC-1), 0.83 MN (AC-2), and 0.91 MN (AC-3), with AC-3 showing 1.1 and 0.1 times increases. These multipliers remain relatively stable at higher intensities (2.5 and 0.1 times at $a_{max} = 1.2g$), unlike the amplified differences observed for $|M|_{max}$. The COV of $|M|_{max}$ and N_{max} in AC-2/AC-3, considering seismic uncertainty, showed an increasing trend between $0.2g$ and $0.4g$, followed by a gradual decrease, with relatively uniform differences. However, the COV of $|M|_{max}$ and N_{max} under AC-1, which only considers rock mass properties' spatial variability, exhibited a slow increasing trend. $|V|_{max}$ response demonstrates unique characteristics compared to $|M|_{max}$ and N_{max} when examining uncertainty effects. Under AC-3, the mean of $|V|_{max}$ shows progressive amplification that diminishes with increasing a_{max}, initially exceeding the AC-1 by 2.7 times at $0.2g$, reducing to 2.1 times at $1.2g$, while maintaining a more modest 1.26 to 1.06 times increase over the AC-2. When uncertainty of earthquake excitation is considered, the COV for $|V|_{max}$ demonstrates a consistent decreasing trend as a_{max} increases. This behavior contrasts with the non-monotonic variability patterns observed for $|M|_{max}$ and N_{max} under similar conditions. Conversely, the COV of $|V|_{max}$ under AC-1 shows a gradual increase with rising a_{max}, mirroring the trend seen for $|M|_{max}$ and N_{max}.

To quantify the reliability of tunnels under different a_{max} conditions, Fig. 16 shows the P_f values of $|M|_{max}$, N_{max}, $|V|_{max}$, and tunnel system under different ACs at various a_{max} values. The P_f analysis yields the following quantitative results for different loading conditions: Under $a_{max} = 0.2g$, $|M|_{max}$ shows P_f values of 0% (AC-1), 1.4% (AC-2), and 1.8% (AC-3), while N_{max} shows P_f values of 0% (AC-1), 0% (AC-2), and 0.2 % (AC-3), and $|V|_{max}$ exhibits P_f values of 0% (AC-1 and 2) and 0.2% (AC-3). At the higher intensity of $a_{max} = 1.2g$, these values increase substantially: $|M|_{max}$ reaches 58% (AC-1), 88% (AC-2), and 96% (AC-3); N_{max} rises to 5% (AC-1), 9% (AC-2), and 12% (AC-3); and $|V|_{max}$ climbs to 15% (AC-1), 35% (AC-2), and 40% (AC-3). The data reveal consistent patterns where M maintains the highest failure probabilities across all conditions, N shows the lowest risk, and V occupies an intermediate position. Notably, the system failure probabilities closely mirror those of M, confirming that bending resistance governs overall tunnel safety under seismic loading, with seismic uncertainty representing the dominant risk contributor whose influence intensifies progressively with increasing a_{max}. While rock mass properties' spatial variability introduces secondary effects, its interaction with seismic uncertainty becomes increasingly critical

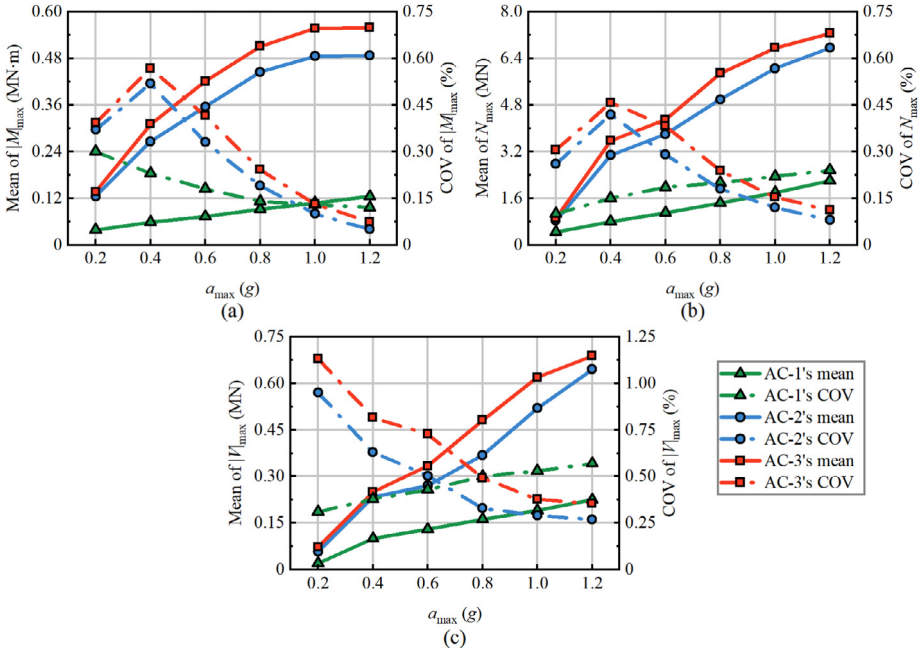

Fig. 15. Mean and COV of the mechanical behavior of lining under different a_{max}. (a) Mean and COV of $|M|_{max}$, (b) mean and COV of N_{max}, and (c) mean and COV of $|V|_{max}$.

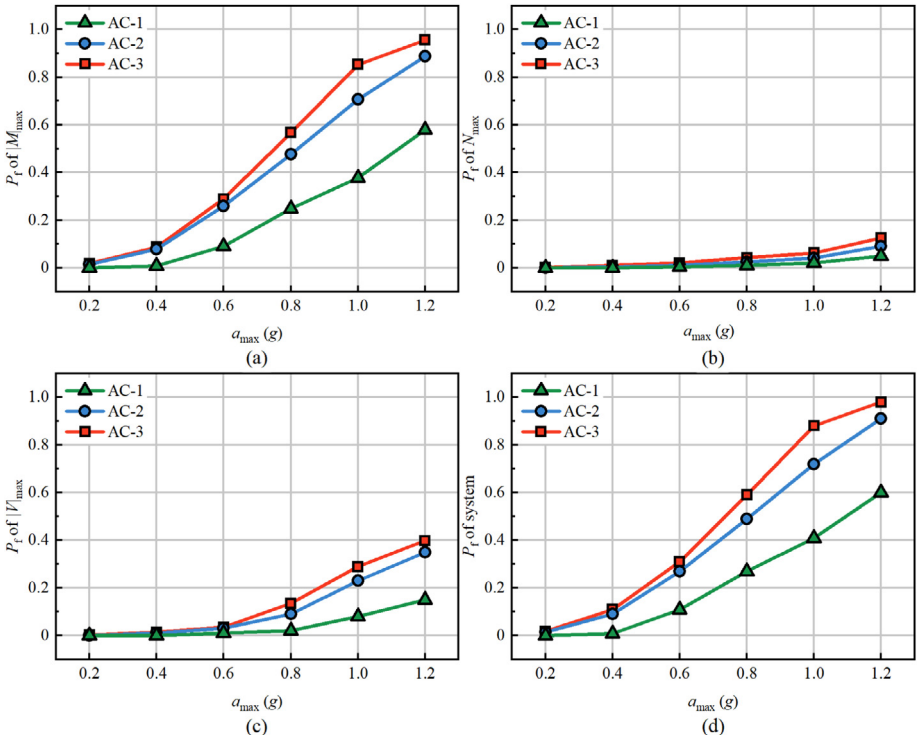

Fig. 16. P_f of the mechanical behavior of lining under different a_{max}. (a) P_f of $|M|_{max}$, (b) P_f of N_{max}, (c) P_f of $|V|_{max}$, and (d) P_f of the system.

in high-intensity regions, generating P_f that surpasses predictions from single-factor analyses. These findings provide evidence that seismic design for tunnels in high-intensity areas must necessarily incorporate both uncertainty of rock mass properties and earthquake excitations to ensure adequate safety.

5 Conclusions

This study presents a probabilistic framework for assessing tunnel seismic performance by simultaneously considering the spatial variability of rock mass properties and earthquake excitation uncertainty. The methodology integrates three components: (1) K–L expansion approach combined with MLE and squared exponential ACF to generate realistic random fields of rock mass properties, (2) improved C–P power spectrum model coupled with random function theory to simulate non-stationary earthquake excitations, and (3) statistical characteristics and failure probabilities analysis of mechanical behavior of lining (M, N, V). The framework's applicability is extended through systematic parameter studies of critical seismic parameters (ω_0, ξ_0, a_{max}), providing quantitative insights into their influence on structural response. The significant findings are described below:

(1) A random seismic response of lining structures comparison was conducted between double random factors and a single random factor. Dual random approach yields mean value increases of 251.3% for M, 107.8% for N, and 278.9% for V relative to rock mass parameters-only analyses. Corresponding COV increases of 30.1% (M), 194.2% (N), and 262.8% (V) under double random factors. When compared to earthquake excitation-only conditions, the maximum additional increases reach 24.1% for mean values and 19.3% for COV. Therefore, when both random factors are considered, the randomness of earthquake excitations is the primary influencing factor.

(2) When considering the uncertainty of earthquake excitation, the response results of tunnels do not follow the traditional normal distribution, which increases the difficulty of seismic design for tunnel structures. The uncertainty of rock mass parameters increases the range of dispersion of the results. Therefore, to obtain more reliable random response analysis results, it is necessary to consider both the uncertainty of rock mass and the uncertainty of earthquake excitation.

(3) ω_0 and ξ_0 significantly affect tunnel seismic response characteristics. Increasing these parameters reduces both the mean (up to 83.5% reduction for ω_0, 70% for ξ_0) and variability (COV reductions up to 82.5% and 53.1%, respectively) of the mechanical behavior of the lining. This implies that larger ω_0 and ξ_0 values

may underestimate the failure risk of tunnel linings. Therefore, design practice should adopt the lower bounds of acceptable ω_0 and ξ_0 ranges to ensure adequate safety margins.

(4) a_{max} exhibits a direct positive correlation with the mean value of the mechanical behavior of the lining, while demonstrating distinct variability characteristics across different force components. The analysis reveals that the COV of M and N reaches a peak at $0.4g$ before decreasing, whereas V shows continuous COV reduction with increasing a_{max}. Although secondary in influence, rock mass properties' spatial variability interacts significantly with uncertainty of earthquake excitation, producing P_f that exceeds single factor's results by 3%–38%. These results demonstrate that seismic design must incorporate both uncertainty sources, particularly for tunnels in high-intensity seismic zones where their combined effects become most critical.

Several important limitations warrant further investigation to enhance the methodology's comprehensiveness. Future studies should extend the SR method to incorporate: (1) sequential seismic events, (2) near-fault pulse-type ground motions, and (3) oblique SV-wave incidence across diverse geological-topographical conditions to better capture complex wave propagation phenomena. These extensions would significantly improve the method's capability to address the full spectrum of seismic scenarios encountered in engineering practice, particularly for critical infrastructure in complex geological settings. Furthermore, this study did not account for potential inter-parameter correlations among rock mass properties, which could considerably influence the analytical outcomes. To address this limitation, subsequent research should employ more advanced and rigorous methods—such as incorporating Copula theory—to establish random fields that effectively represent interdependent rock mass parameters and capture their inherent dependency structures. It should also be noted that the treatment of stochastic parameters in this work was simplified to enhance computational efficiency. Thus, future studies are encouraged to investigate the implementation of more advanced computational techniques to accelerate the overall analytical process, thereby facilitating a more comprehensive incorporation of uncertainty sources.

Data availability

The data that support the findings of this study are available from the corresponding author upon reasonable request.

CRediT authorship contribution statement

Xiancheng Mei: Writing – review & editing, Writing – original draft, Visualization, Funding acquisition. **Jiajun Wu:** Writing – review & editing, Writing – original draft, Methodology. **Baiyi Li:** Supervision, Funding acquisition. **Zhen Cui:** Supervision, Funding acquisition. **Chong Yu:** Supervision. **Qian Sheng:** Supervision. **Jian Chen:** Supervision.

Declaration of competing interest

The authors declare that they have no known competing financial interests or personal relationships that could have appeared to influence the work reported in this paper.

Acknowledgement

The work is supported by the National Key R&D Programs for Young Scientists (2023YFB2390400), the National Natural Science Foundation of China (Grant Nos. U21A20159, 52079133, and 12441510), the Hubei Provincial Natural Science Foundation of China (2024AFB041), State Key Laboratory of Intelligent Construction and Healthy Operation and Maintenance of Deep Underground Engineering (SDGZK2412), and Seed Fund for Basic Research and Original Innovation of Young Talents of State Key Laboratory of Geomechanics and Geotechnical Engineering Safety (SKLGGES-ZZJJ2503). The authors want to thank all the members who gave us lots of help and cooperation.

References

Alibeikloo, M., Khabbaz, H., & Fatahi, B. (2022). Random field reliability analysis for time-dependent behaviour of soft soils considering spatial variability of elastic visco-plastic parameters. *Reliability Engineering & System Safety, 219*, 108254.

Cacciola, P., & Deodatis, G. (2011). A method for generating fully non-stationary and spectrum-compatible ground motion vector processes. *Soil Dynamics and Earthquake Engineering, 31*(3), 351–360.

Cao, Z., & Wang, Y. (2014). Bayesian model comparison and selection of spatial correlation functions for soil parameters. *Structural Safety, 49*, 10–17.

Chen, F. Y., Wang, L., & Zhang, W. G. (2019). Reliability assessment on stability of tunnelling perpendicularly beneath an existing tunnel considering spatial variabilities of rock mass properties. *Tunnelling and Underground Space Technology, 88*, 276–289.

Chen, P., Geng, P., Chen, J., & Gu, W. (2023). The seismic damage mechanism of Daliang tunnel by fault dislocation during the 2022 Menyuan Ms6.9 earthquake based on unidirectional velocity pulse input. *Engineering Failure Analysis, 145*, 107047.

Chen, X., & Li, J. (2025). Stochastic nonlinear dynamic analysis and system reliability evaluation of RC structures involving spatial variation under stochastic ground motions. *Structural Safety, 114*, 102581.

China Railway Second Design Institute Engineering Group Co., Ltd. (2017). *TB 10003—2016: Code for Design of Railway Tunnel*. Beijing: China Railway Publishing House Co., LTD. (in Chinese).

Ching, J., & Phoon, K. K. (2013a). Probability distribution for mobilised shear strengths of spatially variable soils under uniform stress states. *Georisk: Assessment and Management of Risk for Engineered Systems and Geohazards, 7*(3), 209–224.

Ching, J., & Phoon, K. K. (2013b). Effect of element sizes in random field finite element simulations of soil shear strength. *Computers and Structures, 126*(15), 120–134.

Ching, J., Hu, Y. G., Yang, Z. Y., Shiau, J. Q., Chen, J. C., & Li, Y. S. (2011). Reliability-based design for allowable bearing capacity of footings on rock masses by considering angle of distortion. *International Journal of Rock Mechanics and Mining Sciences, 48*(5), 728–740.

Cui, L., Yang, W. Y., Sheng, Q., Zheng, J. J., & Ali, N. (2024). Deformation behaviour of strain-softening rock mass in tunnels considering deterioration model of elastic modulus. *Geomechanics and Geophysics for Geo-Energy and Geo-Resources, 10*(1), 171.

Deodatis, G. (1996). Non-stationary stochastic vector processes: Seismic ground motion applications. *Probabilistic Engineering Mechanics, 11*(3), 149–167.

Ding, J. Y., Zhou, J. F., & Cai, W. (2023). An efficient variable selection-based Kriging model method for the reliability analysis of slopes with spatially variable soils. *Reliability Engineering and System Safety, 235*, 109234.

Dong, X., Tan, X., Lu, Z., Zhang, P., Zha, F., & Xu, L. (2024). Reliability analysis of two–pile group in spatially variable soil considering differential settlement. *Ocean Engineering, 307*, 118182.

Fenton, G. A., & Griffiths, D. V. (2002). Probabilistic foundation settlement on spatially random soil. *Journal of Geotechnical and Geoenvironmental Engineering, 128*(5), 381–390.

Fenton, G. A., Griffiths, D. V., & Williams, M. B. (2005). Reliability of traditional retaining wall design. *Géotechnique, 55*(1), 55–62.

Guo, X., Du, D., & Dias, D. (2019). Reliability analysis of tunnel lining considering soil spatial variability. *Engineering Structures, 196*, 109332.

Housner, G. W. (1947). Characteristics of strong-motion earthquakes. *Bulletin of the Seismological Society of America, 37*(1), 19–31.

Huang, G., & Chen, X. (2009). Wavelets-based estimation of multivariate evolutionary spectra and its application to nonstationary downburst winds. *Engineering Structures, 31*(4), 976–989.

Huang, H. W., Xiao, L., Zhang, D. M., & Zhang, J. (2017). Influence of spatial variability of soil Young's modulus on tunnel convergence in soft soils. *Engineering Geology, 228*, 357–370.

Institute of Geophysics, China Earthquake Administration, et al. (2015). *GB 18306—2015: Seismic Ground Motion Parameters Zonation of China*. Beijing: China Planning Press. (in Chinese).

Jerez, D. J., Chwala, M., Jensen, H. A., & Beer, M. (2024). Optimal borehole placement for the design of rectangular shallow foundation systems under undrained soil conditions: A stochastic framework. *Reliability Engineering & System Safety, 242*, 109771.

Ji, J., Wang, C. W., Gao, Y. F., & Zhang, L. M. (2021). Probabilistic investigation of the seismic displacement of earth slopes under stochastic ground motion: A rotational sliding block analysis. *Canadian Geotechnical Journal, 58*(7), 952–968.

Jiang, S., Li, D., Phoon, K. K., Cao, Z., & Zhou, C. (2015). Efficient system reliability analysis of slope stability in spatially variable soils using Monte Carlo simulation. *Journal of Geotechnical and Geoenvironmental Engineering, 141*(2), 04014096.

Johari, A., & Rahmati, H. (2019). System reliability analysis of slopes based on the method of slices using sequential compounding method. *Computers and Geotechnics, 114*, 103116.

Johari, A., & Sabzi, A. (2017). Reliability analysis of foundation settlement by stochastic response surface and random finite element method. *Scientia Iranica Transactions A: Civil Engineering, 24*(6), 2741–2751.

Johari, A., Sabzi, A., & Gholaminejad, A. (2019). Reliability analysis of differential settlement of strip footings by stochastic response surface method. *Iranian Journal of Science and Technology-transactions of Civil Engineering, 43*(1), 37–48.

Johari, A., & Fooladi, H. (2022). Simulation of the conditional models of borehole's characteristics for slope reliability assessment. *Transportation Geotechnics, 35*, 100778.

Johari, A., & Talebi, A. (2021). Stochastic analysis of piled-raft foundations using the random finite-element method. *International Journal of Geomechanics, 21*(4), 04021020.

Khosravi-Hajivand, A., & Johari, A. (2024). Unsaturated soil nailing wall system reliability analysis using random finite element. *Computers and Geotechnics, 173*, 106554.

Kroetz, H. M., Do, N., Dias, D., & Beck, A. T. (2018). Reliability of tunnel lining design using the hyperstatic reaction method. *Tunnelling and Underground Space Technology, 77*, 59–67.

Kuhlemeyer, R. L., & Lysmer, J. (1973). Finite element method accuracy for wave propagation problems. *Journal of the Geotechnical Engineering Division, 99*(5), 421–427.

Lee, J., & Fenves, G. L. (1998). Plastic-damage model for cyclic loading of concrete structures. *Journal of Engineering Mechanics, 124*(8), 892–900.

Li, J., Tian, Y., & Cassidy, M. J. (2015). Failure mechanism and bearing capacity of footings buried at various depths in spatially random soil. *Journal of Geotechnical and Geoenvironmental Engineering, 141*(2), 04014099.

Li, J. D., Yang, T. H., Liu, F. Y., Zhao, Y., Liu, H. L., Deng, W. X., Gao, Y., & Li, H. B. (2024). Modeling spatial variability of mechanical parameters of layered rock masses and its application in slope optimization at the open-pit mine. *International Journal of Rock Mechanics and Mining Sciences, 181*, 105859.

Luo, Z., Li, Y., Zhou, S., & Di, H. (2018). Effects of vertical spatial variability on supported excavations in sands considering multiple geotechnical and structural failure modes. *Computers and Geotechnics, 95*, 16–29.

Luo, C. R., & Peng, Y. B. (2024). Stochastic simulation of earthquake ground motions based on improved finite-fault model. *Soil Dynamics and Earthquake Engineering, 176*, 108669.

Marano, G. C., Trentadue, F., Morrone, E., & Amara, L. (2008). Sensitivity analysis of optimum stochastic nonstationary response spectra under uncertain soil parameters. *Soil Dynamics and Earthquake Engineering, 28*(12), 1078–1093.

Mei, X. C., Sheng, Q., Cui, Z., Zhang, M. C., & Dias, D. (2023). Experimental investigation on the mechanical and damping properties of rubber-sand-concrete prepared with recycled waste tires for aseismic isolation layer. *Soil Dynamics and Earthquake Engineering, 165*, 107718.

Ministry of Railways of the People's Republic of China (2006). *GB 50111—2006: Code for seismic design of railway engineering*. Beijing: China Planning Press (in Chinese).

Ministry of Housing and Urban-Rural Development of the People's Republic of China (2010). *GB 50010—2010: Code for Design of Concrete Structures*. Beijing: China Planning Press (in Chinese).

Napoli, M. L., Barbero, M., & Scavia, C. (2021). Tunneling in heterogeneous rock masses with a block-in-matrix fabric. *International Journal of Rock Mechanics and Mining Sciences, 138*, 104655.

Pang, R., Xu, B., Zou, D., & Kong, X. (2018a). Stochastic seismic performance assessment of high CFRDs based on generalized probability density evolution method. *Computers and Geotechnics, 97*, 233–245.

Pang, R., Xu, B., Kong, X. J., Zhou, Y., & Zou, D. G. (2018b). Seismic performance evaluation of high CFRD slopes subjected to near-fault ground motions based on generalized probability density evolution method. *Engineering Geology, 246*, 391–401.

Pang, R., Xu, B., Zhou, Y., & Song, L. F. (2021). Seismic time-history response and system reliability analysis of slopes considering uncertainty of multi-parameters and earthquake excitations. *Computers and Geotechnics, 136*, 104245.

Phoon, K. K., Quek, S. T., & An, P. (2003). Identification of statistically homogeneous soil layers using modified Bartlett statistics. *Journal of Geotechnical and Geoenvironmental Engineering, 129*(7), 649–659.

Renani, H. R., Martin, C. D., Varona, P., & Lorig, L. (2019). Stability analysis of slopes with spatially variable strength properties. *Rock Mechanics and Rock Engineering, 52*(10), 3791–3808.

Singh, D. K., Mandal, A., Karumanchi, S. R., Murmu, A., & Sivakumar, N. (2018). Seismic behaviour of damaged tunnel during aftershock. *Engineering Failure Analysis, 93*, 44–54.

Sun, B., Wang, P., Deng, M., Fang, H., Xu, J., Zhang, S., & Wang, C. (2024). Seismic performance assessment of hydraulic tunnels considering oblique incoming nonstationary stochastic SV waves based on the generalized PDEM. *Tunnelling and Underground Space Technology, 143*, 105481.

Vanmarcke, E. (1983). *Random fields: Analysis and synthesis*. Cambridge: MIT Press.

Wang, L., Cui, G., Zhang, C., Zhao, Y., Ma, J., & Min, B. (2024a). Failure characteristics and seismic behavior of steel basalt hybrid fiber reinforced concrete lining for the tunnel in strong earthquake areas. *Engineering Failure Analysis, 162*, 108357.

Wang, T. T., Kwok, O. L. A., & Jeng, F. S. (2021). Seismic response of tunnels revealed in two decades following the 1999 Chi-Chi earthquake (Mw 7.6) in Taiwan: A review. *Engineering Geology, 287*, 106090.

Wang, Y. B., He, J. J., & Shu, S. (2022). Seismic responses of rectangular tunnels in liquefiable soil considering spatial variability of soil properties. *Soil Dynamics and Earthquake Engineering, 162*, 107498.

Wang, Z. K., Song, Z. Q., Li, C., & Liu, Y. H. (2024b). Random dynamic response analysis of an asphalt concrete core wall dam on deep overburden with double random factors. *Computers and Geotechnics, 171*, 106364.

Wu, Y., Wang, J., Cheng, J., & Yang, S. (2024). Dimension-reduction spectral representation of soil spatial variability and its application in the efficient reliability analysis of seismic response in tunnels. *Reliability Engineering & System Safety, 248*, 110175.

Wu, Y., Zhou, X., Gao, Y., Zhang, L., & Yang, J. (2019). Effect of soil variability on bearing capacity accounting for non-stationary characteristics of undrained shear strength. *Computers and Geotechnics, 110*, 199–210.

Xu, B., Lu, Y. Z., & Pang, R. (2024). Seismic safety assessment of dam slopes considering rockfill softening characteristics, shear strength uncertainties, and stochastic ground motion. *Structures, 62*, 106180.

Xu, B., Wang, G., Peng, R., & Zhou, Y. (2025). Stochastic simulation method for ground motions considering parameters uncertainty of evolutionary power spectral density model for structural reliability assessment. *Mechanical Systems and Signal Processing, 237*, 112941.

Yao, C., He, C., Wang, T., Chen, C., Geng, P., Dong, W., Yuan, F., & Xu, G. (2024). Damages of highway tunnels during 2022 luding earthquake (Mw = 6.6). *Soil Dynamics and Earthquake Engineering, 177*, 108357.

Zhang, H., Luo, F., Yang, S., & Wu, Y. (2023). Probabilistic analysis of crown settlement in high-speed railway tunnel constructed by sequential excavation method considering soil spatial variability. *Tunnelling and Underground Space Technology, 140*, 105342.

Zhang, L., Fredlund, M., Fredlund, D. G., Lu, H., & Wilson, G. W. (2015). Comparison of 2-D and 3-D slope stability analyses for unsaturated soil slopes. *Engineering Geology, 193*, 374–383.

Zhang, S., Wang, Y., Gao, Q., Ma, X., Zhou, H., & Wang, Z. (2024). Probabilistic analysis of ground settlement induced by tunnel excavation in multilayered soil considering spatial variability. *Computers and Geotechnics, 165*, 105951.

Zhang, W., Nagger, M., Ni, P., Zhao, M., & Du, X. (2025). Nonlinear seismic response analysis of underground structures considering spatial variability of soil parameters. *Tunnelling and Underground Space Technology, 159*, 106445.